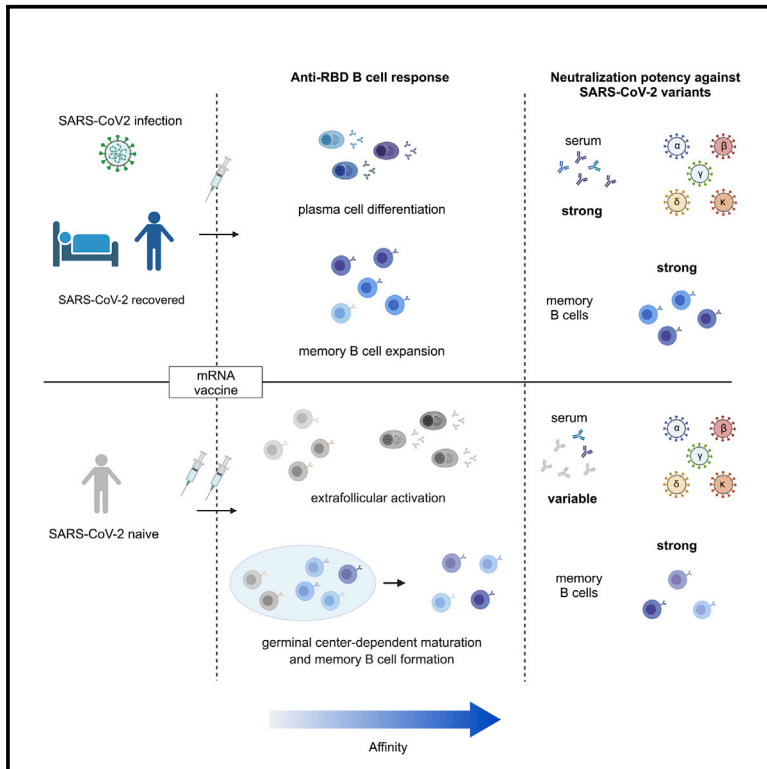


Immunity

mRNA vaccination of naive and COVID-19-recovered individuals elicits potent memory B cells that recognize SARS-CoV-2 variants

Graphical abstract



Authors

Aurélien Sokal,
Giovanna Barba-Spaeth,
Ignacio Fernández, ...,
Claude-Agnès Reynaud,
Pascal Chappert, Matthieu Mahévas

Correspondence

jean-claude.weill@inserm.fr (J.-C.W.),
claudie-agnes.reynaud@inserm.fr (C.-
A.R.),
pascal.chappert@inserm.fr (P.C.),
matthieu.mahevas@aphp.fr (M.M.)

In brief

To better understand B cell responses to SARS-CoV-2 mRNA vaccination, Sokal et al. analyzed memory B cells from COVID-19-recovered and naive individuals. In recovered individuals, vaccination amplifies a broad repertoire of matured MBCs and generates variant-neutralizing plasma cells. In naive individuals, vaccination induces an MBC pool containing potent neutralizing clones against all current variants of concern, including beta and delta.

Highlights

- Vaccination boosts high-affinity RBD memory B cells (MBCs) in COVID-19-recovered patients
- Boosted MBCs retain their diversity and express potent variant-neutralizing antibodies
- SARS-CoV-2-naive individuals show low serum neutralization of variants after vaccination
- Maturation of MBCs in naive individuals allows them to respond to variants of concern



Article

mRNA vaccination of naive and COVID-19-recovered individuals elicits potent memory B cells that recognize SARS-CoV-2 variants

Aurélien Sokal,^{1,2,15} Giovanna Barba-Spaeth,^{3,15} Ignacio Fernández,^{3,15} Matteo Broketa,^{4,14,15} Imane Azzaoui,^{2,5,16} Andréa de La Selle,^{1,2,16} Alexis Vandenberghe,^{2,5,16} Slim Fourati,^{6,7,16} Anais Roeser,^{1,2} Annalisa Meola,³ Magali Bouvier-Alias,^{6,7} Etienne Crickx,^{1,2} Laetitia Languille,² Marc Michel,² Bertrand Godeau,² Sébastien Gallien,⁸ Giovanna Melica,⁸ Yann Nguyen,⁹ Virginie Zarrouk,⁹ Florence Canoui-Poitrine,¹⁰ France Pirenne,^{5,11} Jérôme Mégret,¹² Jean-Michel Pawlotsky,^{6,7} Simon Fillatreau,¹ Pierre Bruhns,^{4,17} Felix A. Rey,^{3,17} Jean-Claude Weill,^{1,17,*} Claude-Agnès Reynaud,^{1,17,*} Pascal Chappert,^{1,13,17,*} and Matthieu Mahévas^{1,2,5,17,18,*}

¹Institut Necker Enfants Malades (INEM), INSERM U1151/CNRS UMS 8253, Université de Paris, Paris, France

²Service de Médecine Interne, Centre Hospitalier Universitaire Henri-Mondor, Assistance Publique-Hôpitaux de Paris (AP-HP), Université Paris-Est Créteil (UPEC), Créteil, France

³Institut Pasteur, Université de Paris, Unité de Virologie Structurale, CNRS UMR 3569, Paris 75015, France

⁴Institut Pasteur, Université de Paris, INSERM UMR 1222, Unit of Antibodies in Therapy and Pathology, Paris 75015, France

⁵INSERM U955, Équipe 2, Institut Mondor de Recherche Biomédicale (IMRB), Université Paris-Est Créteil (UPEC), Créteil, France

⁶Département de Virologie, Bactériologie, Hygiène et Mycologie-Parasitologie, Centre Hospitalier Universitaire Henri-Mondor, Assistance Publique-Hôpitaux de Paris (AP-HP), Créteil, France

⁷INSERM U955, Équipe 18, Institut Mondor de Recherche Biomédicale (IMRB), Université Paris-Est Créteil (UPEC), Créteil, France

⁸Service de Maladies Infectieuses, Centre Hospitalier Universitaire Henri-Mondor, Assistance Publique-Hôpitaux de Paris (AP-HP), Université Paris-Est Créteil (UPEC), Créteil, France

⁹Service de Médecine Interne, Hôpital Beaujon, Assistance Publique-Hôpitaux de Paris, Université de Paris, Clichy, France

¹⁰Département de Santé Publique, Unité de Recherche Clinique (URC), CEpiA (Clinical Epidemiology and Ageing), EA 7376, Institut Mondor de Recherche Biomédicale (IMRB), Centre Hospitalier Universitaire Henri-Mondor, Assistance Publique-Hôpitaux de Paris (AP-HP), Université Paris-Est Créteil (UPEC), Créteil, France

¹¹Etablissement Français du Sang (EFS) Ile de France, Créteil, France

¹²Plateforme de Cytométrie en Flux, Structure Fédérative de Recherche Necker, INSERM US24-CNRS UMS3633, Paris, France

¹³Inovation, Paris, France

¹⁴Sorbonne Université, Collège doctoral, Paris 75005, France

¹⁵These authors contributed equally

¹⁶These authors contributed equally

¹⁷Senior author

¹⁸Lead contact

*Correspondence: jean-claude.weill@inserm.fr (J.-C.W.), claudes-agnes.reynaud@inserm.fr (C.-A.R.), pascal.chappert@inserm.fr (P.C.), matthieu.mahevas@aphp.fr (M.M.)

<https://doi.org/10.1016/j.immuni.2021.09.011>

SUMMARY

In addition to serum immunoglobulins, memory B cell (MBC) generation against severe acute respiratory syndrome coronavirus 2 (SARS-CoV-2) is another layer of immune protection, but the quality of MBC responses in naive and coronavirus disease 2019 (COVID-19)-recovered individuals after vaccination remains ill defined. We studied longitudinal cohorts of naive and disease-recovered individuals for up to 2 months after SARS-CoV-2 mRNA vaccination. We assessed the quality of the memory response by analysis of antibody repertoires, affinity, and neutralization against variants of concern (VOCs) using unbiased cultures of 2,452 MBCs. Upon boosting, the MBC pool of recovered individuals expanded selectively, matured further, and harbored potent neutralizers against VOCs. Although naive individuals had weaker neutralizing serum responses, half of their RBD-specific MBCs displayed high affinity toward multiple VOCs, including delta (B.1.617.2), and one-third retained neutralizing potency against beta (B.1.351). Our data suggest that an additional challenge in naive vaccinees could recall such affinity-matured MBCs and allow them to respond efficiently to VOCs.



INTRODUCTION

The coronavirus disease 2019 (COVID-19) pandemic, caused by severe acute respiratory syndrome coronavirus 2 (SARS-CoV-2), has resulted in more than 220 million infections and at least 4.5 million deaths as of September 6, 2021. Vaccination is the main hope to control the pandemic. COVID-19 vaccines containing nucleoside-modified mRNA encoding the original Wuhan-Hu-1 SARS-CoV-2 spike glycoprotein (S), developed by Pfizer/BioNTech (BNT162b2) and Moderna (mRNA-1273), are now being deployed worldwide. They have been shown to be safe and highly effective to prevent infection and control disease severity (Baden et al., 2021; Dagan et al., 2021; Polack et al., 2020).

The emergence of SARS-CoV-2 variants bearing mutations in key B cell epitopes, however, has raised concerns that virus evolution will erode natural immunity or the protection offered by vaccination. One early mutation in the S protein (D614G), which shifts the equilibrium between the open and closed protein conformation without modifying antibody neutralization, has become globally dominant (Plante et al., 2021; Weissman et al., 2021; Yurkovetskiy et al., 2020), and novel variants of concern (VOCs) or variants of interest (VOIs) have spread around the world, with additional combinations of mutations and deletions located mainly in the ACE-2 receptor-binding domain (RBD) and the N-terminal domain of the S protein. Mutations in the RBD are of particular importance because a large fraction of neutralizing antibodies elicited after infection and vaccination target this domain. The selective advantage provided by these mutations has resulted in their increasing prevalence: N501Y in the B.1.1.7 (alpha) variant; K417N, E484K, N501Y in the B.1.351 (beta) variant; K417T, E484K, N501Y in the P.1 (gamma) variant; and L452R, E484Q, or L452R, T478K in the B.1.617.1 (kappa) and B.1.617.2 (delta) variants, respectively (Cherian et al., 2021; Davies et al., 2021; Greaney et al., 2021a; Tegally et al., 2021).

The higher infectiousness of the B.1.1.7 variant does not impair the neutralizing antibody response (Davies et al., 2021; Garcia-Beltran et al., 2021; Planas et al., 2021a; Supasa et al., 2021). In contrast, the E484K and K417T/N mutations in the B.1.351 and P.1 strains markedly reduced the neutralization potency in COVID-19-recovered or naive vaccinated individuals (Cele et al., 2021; Edara et al., 2021; Greaney et al., 2021a; Hoffmann et al., 2021; Planas et al., 2021a; Wang et al., 2021a; Xie et al., 2021). Even though infection with VOCs or VOIs remains possible after successful vaccination (Hacisuleyman et al., 2021), the effectiveness of the BNT162b2 vaccine against B.1.351 in preventing severe disease has been demonstrated recently during a vaccination campaign in Qatar (Abu-Raddad et al., 2021).

In parallel to the rapid antibody-secreting cell (ASC) and serum immunoglobulin G (IgG) response, progressive generation of memory B cells (MBCs) against the SARS-CoV-2 virus is another layer of immune protection (Dugan et al., 2021; Gaebler et al., 2021; Rodda et al., 2021; Sakharkar et al., 2021; Sokal et al., 2021). MBCs not only persist after infection but evolve continuously and mature by progressive acquisition of somatic mutations in their variable-region genes to improve affinity through an ongoing germinal center response, potentially driven by anti-

genic persistence (Gaebler et al., 2021; Rodda et al., 2021; Sokal et al., 2021). MBCs further drive the recall response after antigenic rechallenge by differentiating into new ASCs displaying the diverse array of high-affinity antibodies contained in the MBC repertoire. However, a strong convergence of the anti-RBD response across COVID-19-recovered and naive vaccinated individuals shaped by recurrent germline gene families has been described. This could favor viral mutational escape because one single mutation in the RBD can confer a selective advantage by reducing the binding and neutralizing activity of antibodies (Garcia-Beltran et al., 2021; Greaney et al., 2021a).

Upon vaccination, COVID-19-recovered individuals showed a striking expansion of RBD-specific MBCs (Goel et al., 2021a; Wang et al., 2021b) and elicited a strong serum antibody response, including cross-neutralizing antibodies against VOCs (Ebinger et al., 2021; Konstantinidis et al., 2021; Krammer et al., 2021; Manisty et al., 2021; Saadat et al., 2021; Samanovic et al., 2021; Stamatatos et al., 2021; Wang et al., 2021b). Much less is known about the long-term stability, dynamics, and functionality of the MBC repertoire after repeated antigenic stimulation. How the MBC pool will contract or expand its diversity after a new challenge is of major importance in the context of vaccination schemes with repeated homologous or heterologous booster doses and coexistence of multiple VOCs.

Here we longitudinally characterized the dynamics, clonal evolution, affinity, and neutralization capacity of anti-SARS-CoV-2 MBCs after mRNA vaccination in naive and SARS-CoV-2-recovered individuals from an analysis of over 2,000 naturally expressed antibodies from single-cell cultured, RBD-specific MBCs. We demonstrate that mRNA vaccination selects high-affinity neutralizing clones without compromising the overall MBC pool.

RESULTS

mRNA vaccination boosts serum IgG levels in SARS-CoV-2-recovered and naive individuals

The B cell immune response elicited by vaccination was analyzed in two cohorts, one of individuals infected previously with SARS-CoV-2 (SARS-CoV-2 recovered) and one of virus-naive individuals (SARS-CoV-2 naive). We previously characterized the longitudinal evolution and maturation, up to 6 months after infection, of SARS-CoV-2-responding B cells in a cohort of mild ambulatory (M-CoV) and severe forms of COVID-19 requiring oxygen (S-CoV) (Sokal et al., 2021). Thirty-four individuals from this original cohort were included in this study, along with 9 additional individuals with COVID-19, for a total of 17 S-CoV and 26 M-CoV individuals (Figure 1A; Table S1). All individuals in this first cohort received one dose of the Pfizer-BioNTech mRNA (BNT162b2) vaccine between 6 and 12 months after infection (median, 309 days after COVID-19 symptom onset; range, 183–362 days; Table S1C). This unique vaccine dose for SARS-CoV-2-recovered individuals is referred to as “boost.” As a parallel cohort, we recruited 25 healthcare workers with no clinical history of COVID-19 and no serological evidence of previous SARS-CoV-2 infection. SARS-CoV-2-naive individuals in this second cohort received 2 doses of the BNT162b2 vaccine as part of the French vaccination campaign. The second vaccine dose, also referred to as “boost,” was received, in

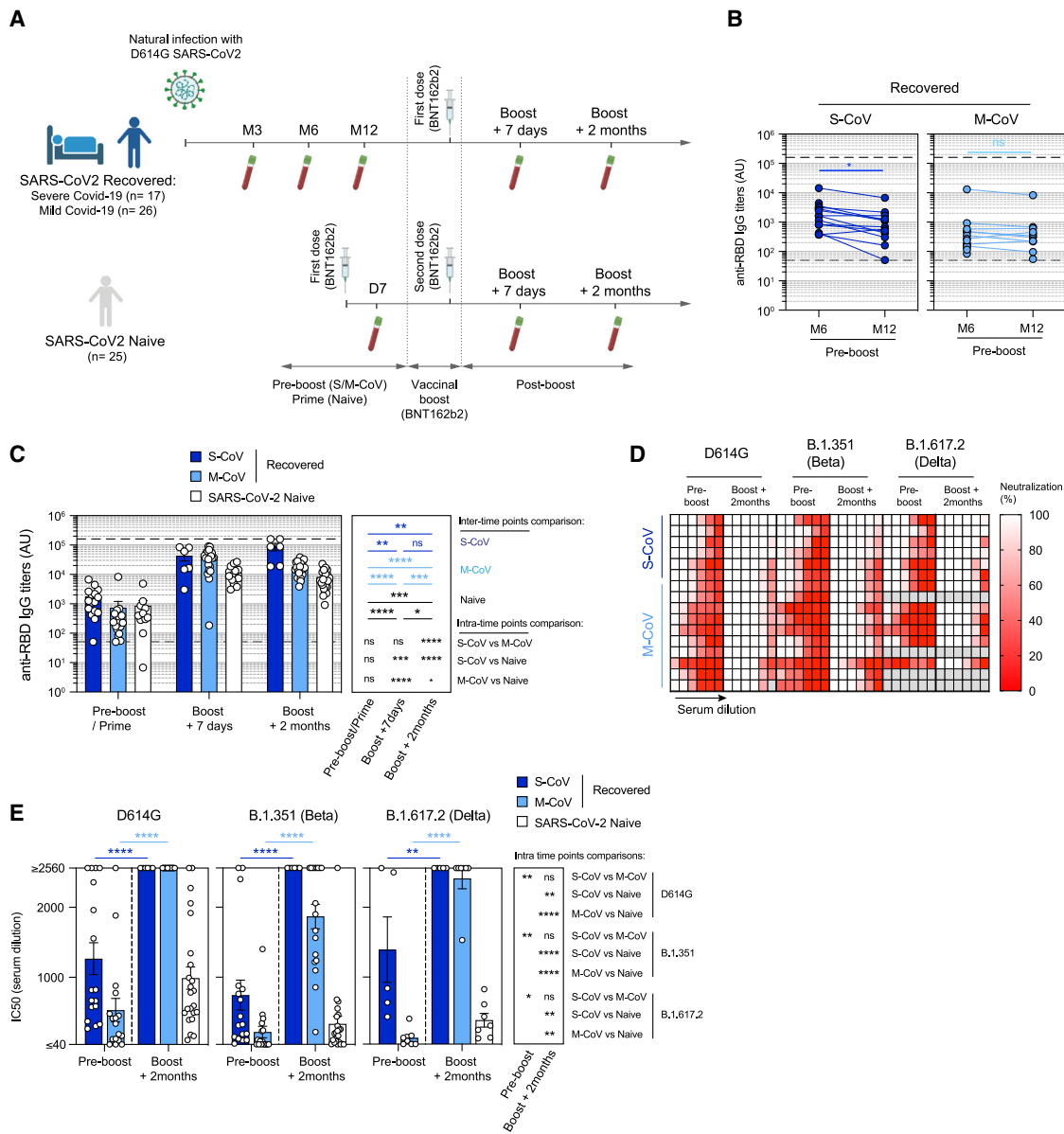


Figure 1. The mRNA vaccine boosts humoral response against SARS-CoV-2 and VOCs in naive and SARS-CoV-2-recovered individuals

(A) Cohort design.

(B) Anti-SARS-CoV-2 RBD serum IgG titers measured by ELISA in S-CoV (n = 16, left panel, dark blue) and M-CoV (n = 15, right panel, light blue) 6 and 12 months after symptom onset.

(C) Evolution of anti-SARS-CoV-2 RBD serum IgG titers after BNT162b2 vaccination. IgG titers (arbitrary units [a.u.]) are shown at pre-boost (month 6 or month 12) for SARS-CoV-2-recovered (S-CoV, dark blue; M-CoV, light blue) or after the prime for naive individuals (white) as well as 7 days and 2 months after the vaccine boost. Bars indicate mean ± SEM.

(B and C) The lower dashed line indicates the positivity threshold, and the upper dashed line indicates the upper limit of detection as provided by the manufacturer.

(D) Heatmap representing the observed *in vitro* neutralization of D614G SARS-CoV-2 (left), B.1.351 (center), and B.1.617.2 VOCs (right) by sera from SARS-CoV-2-recovered individuals at the pre-boost and boost + 2 months time points (serial dilutions: 1/10, 1/40, 1/160, 1/640, 1/2,560, and 1/10,240). Each line represents one individual.

(E) Half-maximal inhibitory concentration (IC₅₀) for all sera tested from SARS-CoV-2-recovered and naive individuals at pre-boost and boost + 2 months time points against D614G SARS-CoV-2, B.1.351, and B.1.617.2 VOCs. Bars indicate mean ± SEM.

We performed two-way ANOVA with multiple comparisons of all groups (B), repeated-measures mixed-effects model analysis with two sets of multiple comparisons (between donor groups inside each time point and between time points for each donor group) (C), and repeated-measures mixed-effects model analysis with multiple comparisons between time points for each recovered donor group and Kruskal-Wallis with multiple comparisons between donor groups inside each time point (E) (Benjamini, Krieger, and Yekutieli false discovery rate [FDR] correction was used for all multiple comparisons). ****p < 0.0001, ***p < 0.001, **p < 0.01, *p < 0.05. See also Figure S1 and Tables S1 and S2.

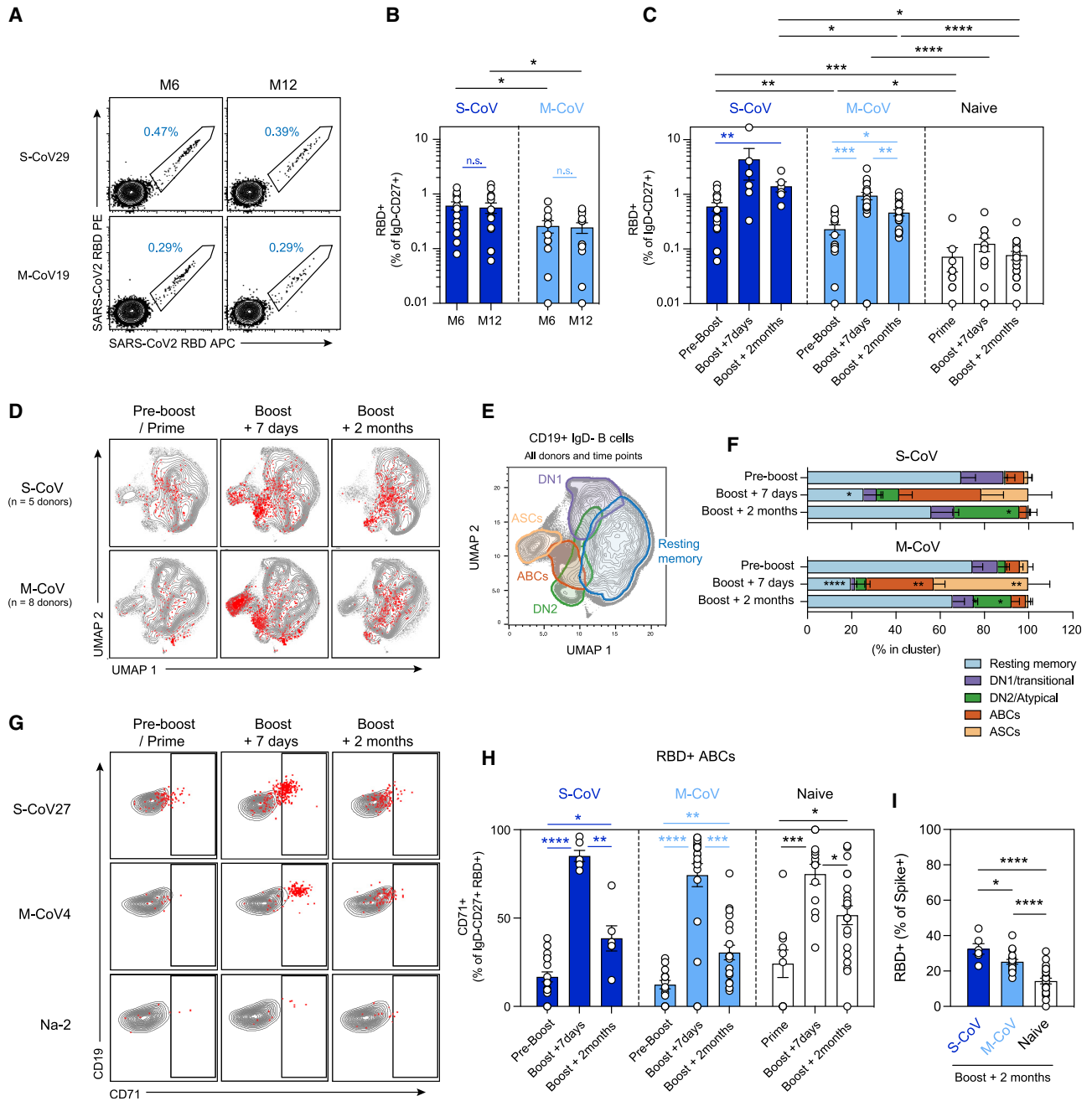


Figure 2. mRNA vaccination activates multiple SARS-CoV-2 RBD-specific B cell subsets in SARS-CoV-2-recovered and naive individuals
 (A) Representative dot plot of SARS-CoV-2 RBD staining of CD19⁺IgD⁻CD27⁺CD38^{int/low} MBCs at 6 and 12 months in one S-CoV and one M-CoV representative individual.
 (B and C) Frequencies of SARS-CoV-2 RBD-specific cells in live CD19⁺IgD⁻CD27⁺CD38^{int/low} MBCs 6 and 12 months after symptom onset in SARS-CoV-2-recovered individuals (S-CoV: dark blue, n = 14/14; M-CoV: light blue, n = 11/12) (B) and at pre-boost, boost + 7 days, and boost + 2 months time points in S-CoV (dark blue, n = 17/6/6), M-CoV (light-blue, n = 14/21/20), and naive (white, n = 10/13/23) individuals. Bars indicate mean ± SEM.
 (D) UMAP projections of concatenated CD19⁺IgD⁻ B cells multiparametric fluorescence-activated cell sorting (FACS) analysis from 5 S-CoV and 8 M-CoV individuals, analyzed longitudinally. His-tagged labeled SARS-CoV-2 RBD-specific cells are overlaid as red dots.
 (E and F) Unsupervised clustering (FlowSOM) performed on the concatenated FACS dataset. Main defined clusters (>2% of total CD19⁺IgD⁻ B cells) are shown as overlaid contour plots on the global UMAP representation (E). Cluster distribution of SARS-CoV-2 RBD-specific cells in identified clusters, at the indicated time point, is further displayed as bar plots (F). Bars indicate mean ± SEM.
 (G) Representative dot plots for CD71 and CD19 expression in IgD⁻CD19⁺CD38^{int/low} B cells at the indicated time points from representative S-CoV, M-CoV, and naive individuals. SARS-CoV-2 RBD-specific MBCs are overlaid as red dots.

(legend continued on next page)

median, 28 days after the first dose of the vaccine, referred to as “prime.” Post-boost blood samples were collected from all vaccinated participants, in median, 8 days (range, 5–22 days) and 2 months after the injection (Figure 1A; Table S1C). Eight SARS-CoV-2-naive donors were sampled additionally after initial priming.

We first measured the pre- and post-boost evolution of IgG serum titers against the wild-type (WT) RBD in both cohorts. Anti-RBD IgG titers remained stable between 6 and 12 months after infection in SARS-CoV-2-recovered individuals, with only a mild decrease seen in S-CoV individuals (Figure 1B). In line with previous reports, a single dose of mRNA vaccine elicited a strong recall response in all individuals, with anti-RBD IgG titers increasing, on average, by 24-fold in S-CoV and 53-fold in M-CoV individuals compared with pre-boost titers (Figures 1C and S1A; Table S2A). In SARS-CoV-2-naive individuals, the mRNA vaccine boost also induced a robust anti-RBD IgG response (average of 25-fold-increase), although titers remained inferior to SARS-CoV-2-recovered individuals at all time points (mean 10,870 versus 75,511 a.u./mL in S-CoV and 55,024 in M-CoV, $p = 0.005$ and $p < 0.0001$, respectively). Despite contraction of the response in all groups, anti-RBD IgG titers were at least 10-fold higher than pre-boost/prime titers 2 months after boost (Figures 1C and S1A).

Twelve months after infection, all sera from SARS-CoV-2-recovered individuals demonstrated neutralization potential in a focus reduction assay against an authentic SARS-CoV-2 virus carrying the dominant D614G amino acid change in the S1 domain of its S protein (Figures 1D, 1E, S1B, and S1C). This potential was more pronounced in S-CoV than in M-CoV individuals but, as expected, was reduced similarly in both groups against the B.1.351 VOC strain, harboring three mutations in its RBD (N501Y, which increases the affinity for the ACE2 receptor, and E484K and K417N, which are implicated in escape from neutralizing antibodies; Harvey et al., 2021), along with several mutations in other S domains. As reported previously (Goel et al., 2021a; Reynolds et al., 2021; Stamatatos et al., 2021; Wang et al., 2021b), a boost mRNA vaccine strongly enhanced the overall neutralizing potency of SARS-CoV-2-recovered individuals against the D614G and B.1.351 viruses, with all S-CoV and M-CoV sera achieving a half-maximal inhibitory concentration (IC_{50}) lower than 1/2,560 for the D614G strain. All sera from S-CoV individuals also reached strong neutralizing potency against the B.1.351 and B.1.617.2 (delta) virus ($IC_{50} < 1/2,560$), although we cannot exclude differences above the tested dilution range for both VOCs (Figures 1D, 1E, and S1B; Table S2B). For M-CoV individuals, the gain in neutralization potency against B.1.351 and B.1.617.2 VOCs was also clear but more modest for the B.1.351 virus. Sera from all naive individuals also showed detectable neutralizing activity against the D614G strain at the final time point in our study (mean IC_{50} , 1/988; range, <2,560 to 1/103), but never reached the IC_{50} seen in

SARS-CoV-2-recovered individuals. This potency was reduced further against the B.1.351 VOC strain (mean IC_{50} , 1/332), with 8 of 23 individuals (35%) displaying an IC_{50} above 1/100 against this variant. In contrast, all naive individuals tested displayed low but detectable neutralization capacity against the B.1.617.2 variant.

These data show that a boost of mRNA vaccine based on the Wuhan-Hu-1 S protein induces a strong recall response in all SARS-CoV-2-recovered individuals, with strong neutralizing IgG serum titers against D614G SARS-CoV-2 as well as B.1.351 and B.1.617.2 VOCs in most individuals. The lower neutralization potency achieved in naive individuals suggests a key role of the matured MBC pool present in SARS-CoV-2-recovered patients in modeling the quality of the vaccine response, including cross-neutralization of VOCs.

mRNA vaccination mobilizes MBCs in SARS-CoV-2-recovered individuals

Similar to the serum IgG titers, the percentage of RBD-specific and S-specific $CD27^+IgD^-$ B cells remained stable between 6 and 12 months in SARS-CoV-2-recovered individuals irrespective of initial disease severity, confirming generation of germinal center-derived, long-lived MBCs after natural infection (Figures 2A, 2B, S2A, and S2B). RBD-specific MBCs, which represent a large fraction of the neutralizing MBC pool against SARS-CoV-2, expanded substantially after one dose of the mRNA vaccine before a modest contraction at 2 months (Figures 2C and S2C; Table S2). In contrast, only low numbers of RBD-specific B cells were detectable in naive individuals after prime, with a non-significant effect of boost vaccination (Figure 2C), although RBD-specific ASCs were observed in all donors in the early steps of the post-boost response (Figure S2D). The frequency of RBD-specific MBCs persisting 2 months after the boost in naive individuals remained significantly lower than the frequency of MBCs observed in SARS-CoV-2-recovered individuals before vaccination (Figure 2C), with similar profiles observed for S-specific MBCs (Figure S2E). The overall frequency of S-specific MBCs in naive individuals 2 months after the boost (3 months after the prime) even appeared to be reduced compared with the 3-month post-infection time point in SARS-CoV-2-recovered individuals (Figure S2F).

Unsupervised analysis of $CD19^+IgD^-$ switched B cell populations, using a multiparametric flow panel we used previously to describe the initial response against SARS-CoV-2 in these individuals (Sokal et al., 2021), showed that RBD-specific cells mostly resided in the $CD21^+CD27^+IgD^-CD38^{int/+}CD71^{int/-}$ resting MBC compartment before vaccination (Figures 2D–2F; Tables S2C and S2D). These cells switched rapidly to a $CD27^+CD38^{int/+}CD71^+$ activated B cell phenotype (ABC cluster) in the first 7 days after the boost, together with emergence of a population of $RBD^+CD38^{high}CD27^{high}$ ASCs. The persistent expression of the BCR on the surface of these cells

(H) Frequencies of SARS-CoV-2 RBD-specific cells displaying an ABC ($CD19^+CD27^+IgD^-CD71^+$) phenotype at the indicated time points.

(I) Proportion of S-specific MBCs recognizing the RBD in each individual at the 2-month time point. Bars indicate mean \pm SEM.

We performed two-way ANOVA with multiple comparisons of all groups (B), repeated-measures mixed-effects model analysis with two sets of multiple comparisons (between donor groups inside each time point [black lines] and between time points for each donor group [colored lines]) (C and H), and ordinary one-way ANOVA (I) (Benjamini, Krieger, and Yekutieli FDR correction was used for all multiple comparisons). Only significant comparisons are highlighted in (C), (H), and (I). *** $p < 0.0001$, ** $p < 0.001$, * $p < 0.01$, * $p < 0.05$. See also Figure S2 and Table S2.

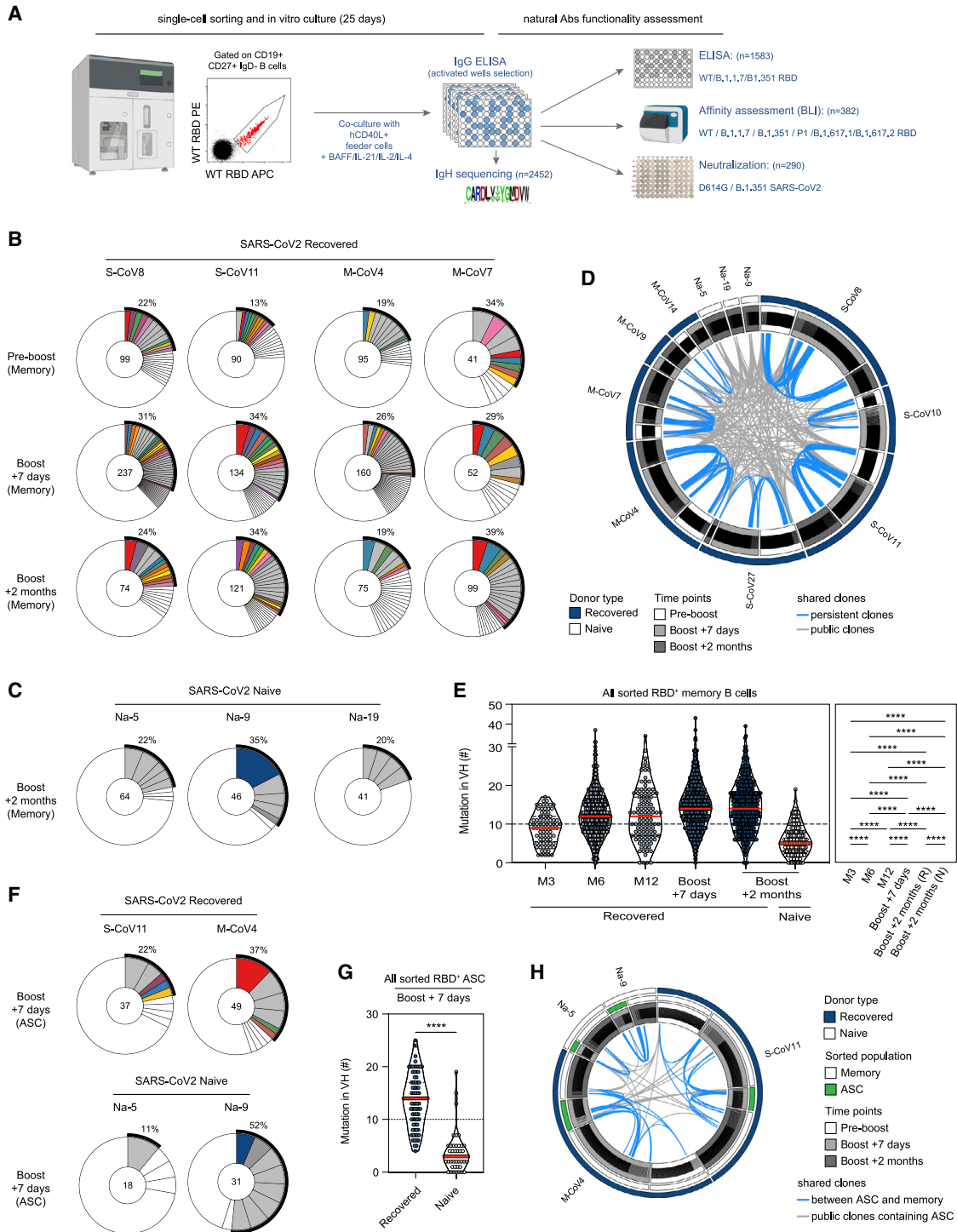


Figure 3. mRNA vaccination elicits a diverse RBD-specific MBC repertoire in SARS-CoV-2-recovered and naive individuals

(A) Experimental scheme for functional assessment of naturally expressed monoclonal antibodies from RBD-specific MBCs. (B and C) Pie charts representing the clonal distribution of RBD-specific MBCs sorted from 2 S-CoV and 2 M-CoV individuals at the pre-boost, boost + 7 days, and boost + 2 months time points (B) and 2 naive individuals at boost + 2 months (C). Clonal representation is depicted according to Wang et al. (2021b): colored slices indicate an expanded MBC clone (2 or more sequences at a given time point) found at several time points in the same individual (persistent clone) or in clonal relationship with ASCs at boost + 7 days, gray slices indicate an expanded MBC clone found at a single time point, and white slices indicate unique sequences found at several time points. The main white sector in each pie chart represents unique sequences observed at a single time point. The outer black semi-circular line indicates the proportion of sequences belonging to expanded clones at a given time point. The total number of sequences is indicated at the pie center.

(legend continued on next page)

harboring a classical ASC phenotype suggests that they were mainly newly generated plasmablasts. These activated subsets contracted progressively and matured as resting MBCs at the latest time point in our study. Atypical MBCs (DN2; IgD⁻CD27^{+/-}CD11c⁺) and ASC precursors (DN1; IgD⁻CD27⁻) RBD-specific clusters were also observed, with a small DN2 fraction persisting up to 2 months after boost, notably in S-CoV individuals (Figure 2F).

The low numbers of RBD-specific B cells in naive individuals precluded a robust unsupervised analysis, and we therefore characterized the phenotype of RBD-specific MBCs from the whole cohort using manual gating, based on the CD19 and CD71 expression profiles, to delineate ABCs (CD19^{high}CD71⁺) (Ellebedy et al., 2016) and resting MBCs (CD19⁺CD71^{low}) among RBD-specific cells over time. A large fraction of RBD-specific MBCs acquired a CD19^{high}CD71⁺ ABC phenotype in the days following the boost in naive individuals, similarly to M-CoV and S-CoV patients (Figures 2G and 2H; Table S2E), demonstrating that vaccine induced a robust expansion of an RBD-specific ABC population in all groups of donors.

The proportion of RBD-specific ABCs decreased over time, favoring an increase of RBD-specific resting MBCs consistent with the contraction of the vaccine response. This contraction appeared to be more pronounced in SARS-CoV-2-recovered individuals, suggesting persistence of GC output in naive individuals (Figure 2H). Similar kinetics were observed for S-specific B cells (Figure S2G), although it should be noted that RBD-specific B cells still represented a smaller proportion of S-specific cells in naive than in SARS-CoV-2 recovered individuals at the 2-month time point (Figures 2I and S2H).

mRNA vaccination maintains the overall diversity of the MBC repertoire

To address how mRNA vaccine boost affects the MBC repertoire, we performed single-cell sorting and culture of RBD-specific MBCs before and 7 days and 2 months after the boost in SARS-CoV-2-recovered individuals and 2 months after the boost in naive individuals (Figure 3A). We obtained a total of 2,452 V_H sequences from 4 S-CoV, 4-M-CoV, and 3 naive individuals (Tables S1D and S3A–S3H). Clonally expanded RBD-specific MBCs were found before vaccination in all SARS-CoV-2-recovered individuals, representing 13%–34% of total V_H sequences for each donor (Figures 3B and S3A). Vac-

cine-activated MBCs showed no evidence of further clonal dominance and conserved their overall diversity despite the major increase in their numbers. The fraction of the repertoire belonging to these clones varies from 19%–39% and remains comparable during contraction, with clones persisting over the pre/post-vaccination period observed in all SARS-CoV-2-recovered individuals. This overall clonal stability was reflected by similar Shannon entropy values at all studied time points (Figure S3B). Similar clonal expansion was observed in naive individuals (Figure 3C), who also harbored a high frequency of convergent RBD-specific clones with SARS-CoV-2-recovered individuals based on immunoglobulin heavy chain (IgH) variable, diversity, and joining (VDJ) sequences (Figure 3D).

We previously reported a progressive accumulation of somatic mutations in RBD-specific clones up to 6 months after infection in this cohort of SARS-CoV-2-recovered individuals (Sokal et al., 2021). The number of mutations in RBD-specific V_H sequences remained stable between 6 and 12 months. In contrast, V_H mutation numbers were increased shortly after the boost and maintained in the MBC pool 2 months thereafter (Figure 3E). This evolution in mutation profile could be confirmed at the individual level for 2 individuals with complete follow-up from 3 or 6 months after symptom onset to 2 months after boost (Figures S3C and S3D; Table S3A). This rapid increase in overall mutational load suggests that a fraction of matured, pre-existing MBCs was mobilized selectively upon vaccine response and persisted over time.

RBD-specific MBCs from naive individuals obtained 2 months after the boost harbored low mutation numbers in their V_H genes, consistent with recruitment of naive B cells in the early phase of the vaccine response. It should also be noted that MBCs from naive individuals harbor an even lower mutational load than MBCs from SARS-CoV-2-recovered individuals at a similar 3-month time point after natural infection (Figure 3E). This suggests that natural infection might drive a faster maturation process of the MBC response.

RBD-specific ASCs from SARS-CoV-2-recovered individuals sorted 7 days after the boost showed clonal relationships with MBCs and highly mutated V_H sequences (Figures 3F–3H and S2A; Tables S3F and S3H). In contrast, RBD-specific ASCs from naive individuals displayed near-germline V_H sequences corresponding to recruitment of naive B cells in the extrafollicular response (Figure 3G). Overall, these results show that activation

(D) Circos plot showing clonal relationships between all sequenced RBD-specific MBCs grouped by donors and time points. Blue lines connect persistent clones, and gray lines connect clones shared by at least two donors (public clones).

(E) Violin plots showing the number of mutations in the V_H segment of RBD-specific MBCs at successive time points in SARS-CoV-2-recovered (month 3, 81 sequences; month 6, 600; month 12, 109; boost + 7 days, 930; boost + 2 months, 430) and naive donors (boost + 2 months, 151). The red line indicates the median.

(F) Pie chart representing the clonal distribution of RBD-specific ASCs sorted for 2 SARS-CoV-2-recovered and 2 naive individuals at boost + 7 days. Colored slices indicate a clone in clonal relationship with an expanded MBC clone from the same donor, gray slices indicate an expanded ASC clone not found in MBCs from the same donor, and white slices indicate unique ASC sequences in a clonal relationship with a non-expanded MBC clone. The outer black semi-circular line indicates the proportion of sequences belonging to expanded ASC clones. The total number of sequences is indicated at the pie center.

(G) Violin plots showing the number of mutations in the V_H segment of RBD-specific ASCs sorted from 2 SARS-CoV-2-recovered (n = 86 sequences) and 2 naive donors (n = 49 sequences) at boost + 7 days. The red line indicates the median.

(H) Circos plot showing clonal relationships between RBD-specific MBCs (white mid-semicircular slice) and RBD-specific ASCs (green mid-semicircular slice) sorted at boost + 7 days from 2 SARS-CoV-2-recovered (one S-CoV, one M-CoV, dark blue outer circular slice) and 2 naive (white outer circular slice) individuals. Blue lines indicate shared clones between ASCs and MBCs, and gray lines indicate public clones containing ASCs.

Ordinary one-way ANOVA with multiple comparisons (Benjamini, Krieger, and Yekutieli FDR correction) (G) and a two-tailed Mann-Whitney test (E) were performed (****p < 0.0001). See also Figure S3 and Table S2.

of the previously matured pool of MBCs by the mRNA vaccine does not bias the clonal diversity of their repertoire in previously infected individuals while selectively amplifying MBCs with a higher mutation load.

MBCs mobilized by mRNA vaccine contain high-affinity clones against VOCs

To determine the potency of the MBC compartment mobilized or elicited by mRNA vaccine against the main natural RBD variants, we first performed ELISA on 1,583 supernatants from single-cell culture of sorted RBD-specific MBCs from 4 S-CoV, 4 M-CoV, and 3 naive individuals (Figure 4A). To normalize for IgG concentration in culture supernatants, we plotted ELISA optical density (OD) values for WT (Wuhan) versus B.1.1.7 or B.1.351 RBD variants. Almost all supernatants similarly recognized the WT and B.1.1.7 RBD, but 20% of them showed a 10-fold decrease in B.1.351 RBD recognition, with similar frequencies of affected supernatants in SARS-CoV-2-recovered and naive individuals (Figures 4A and 4B; Table S2F).

We next assayed the affinity of MBCs against the B.1.1.7, B.1.351, P1, B.1.617.1, and B.1.617.2 RBD variants using biolayer interferometry (BLI), in which naturally expressed monoclonal IgG from single-cell culture supernatants were loaded on anti-human IgG biosensors (Figure S4A). Monoclonal antibodies expressed by MBCs from recovered individuals were highly enriched for high affinity binders against the WT RBD compared with naive patients ($73.9\% \pm 5.8\%$ versus $46.5\% \pm 4.3\%$, $p < 0.01$; Figures 4C and 4D; Table S2G), and comparable frequencies were observed against the B.1.1.7 variant. However, overall affinity profiles were no longer different between recovered and naive donors when the B.1.351, P1, B.1.617.1, or B.1.617.2 variants were tested, with approximately 20%–25% of clones with no or low affinity ($K_D > 10^{-8}$ M) in both groups (Figures 4C, 4D, S4B, and S4C). Somatic hypermutation of V_H genes and antigen-driven affinity maturation against the WT RBD accounts for the higher frequency of high-affinity binders ($K_D < 10^{-9}$ M) in SARS-CoV-2-recovered compared with naive individuals (Figures 4E and 4F). As expected, the number of V_H mutations showed reduced correlation with affinity against the B.1.351 RBD (Figures 4E and 4F), in line with selection of these clones against the WT and not the mutated RBD during the GC maturation process.

Two-by-two comparisons of binding affinities between the WT and the different RBD variants allowed us to validate the sensitivity of our approach with nearly all B.1.351-affected monoclonal antibodies (2-fold increase in variant K_D compared with WT K_D) also affected in their binding of the P.1 RBD variant sharing a similar set of mutations (N501Y, E484K, and K417T/N) but not of the B.1.1.7 RBD variant, which only harbors the N501Y mutation (Figures 5A and 5B). Additional comparisons with B.1.617.1 and B.1.617.2 RBD variants, which harbor the L452R mutation in addition to E484Q for B.1.617.1 and T478K for B.1.617.2 but not the K417N/T mutation, further revealed cases of antibodies affected in their binding to one or more RBD variants (Figures S5A–S5D). Overall, the natural distribution of mutations in the various VOC RBDs (Figures 5C and 5D) allowed us to predict the identity of key binding amino acid residues (i.e., N501, K417, E484, L452, and T478) within the RBD for 164 of 382 tested MBC-derived monoclonal antibodies (Figures

5C–5E). Antibodies affected in their recognition of the B.1.351.1, P.1, and B.1.167.1 RBD were identified as binding to E484, with some antibodies using E484 and L452 for binding, as illustrated by the three-dimensional structure of the RBD (Figures 5C–5E and S5A–S5D). In agreement with a recent structural study (Yuan et al., 2021), clones recognizing the K417 residue were highly enriched for the IGHV3–53 and 3–66 genes, whereas clones recognizing the E484K/Q residue were mostly enriched for the IGHV1–2 and 1–69 genes (Figure S5E; Table S2H). These results also allowed us to ascribe RBD binding residues of B cells within individual MBC repertoires of naive and recovered individuals, confirming the major targeting of the E484 and/or L452 residues within the vaccine-activated pool (Figure 5E), but also highlighting significant inter-donor variability in the overall recognition profile of the SARS-CoV-2 RBD by the MBC repertoire.

Affinity maturation and clonal diversity support B.1.351 neutralization by MBCs

Finally, to evaluate the cross-neutralization potential of RBD-specific clones mobilized after vaccination, 279 randomly selected single MBC culture supernatants from S-CoV, M-CoV, and naive vaccinated individuals were tested in our focus reduction neutralization assay against authentic D614G and B.1.351 SARS-CoV-2 viruses. The majority of RBD-specific MBC clones efficiently neutralized D614G, but a higher frequency of non-neutralizing clones was observed in naive compared with recovered individuals (Figures 6A and S6A; Table S2I). Among potent D614G neutralizers, 40%–60% of monoclonal antibodies efficiently neutralized B.1.351, without a quantitative difference between M-CoV and naive individuals (Figure 6B) or clear association with the V_H mutational load or binding affinity to the WT RBD (Figures 6C and S6A). Nonetheless, potent neutralizing MBC-derived monoclonal antibodies could be detected in all analyzed donors, including SARS-CoV-2-naive vaccinees (ranging from 5%–60% of the overall repertoire in the different donors; Figure S6B).

Loss of affinity against the B.1.351 RBD mainly affected potent D614G neutralizers (Figure 6D), highlighting the strong evolutionary pressure at the virus level to selectively evade this part of the immune response. Plotting K_D values for the WT versus B.1.351 RBD among potent D614G neutralizers further revealed four different profiles correlated with B.1.351 neutralization (Figure 6E); clones could be classified according to whether they retained a similar affinity for binding the B.1.351 RBD compared with the WT one (white and gray sectors, respectively; the gray sector corresponds to lower affinities). Among these two categories, clones could be further divided according to whether they retained neutralization potency against the B.1.351 virus (white and red dots, respectively). Accordingly, MBC-derived monoclonal antibodies displaying similar affinities against the WT and B.1.351 RBD (white sector in Figure 6E) were enriched in strong neutralizers against the B.1.351 variant (white dots), but a subset of these antibodies did display reduced neutralization potency (red dots in the white sector, Figure 6F). These monoclonal antibodies, however, showed a selectively reduced affinity against the whole B.1.351 S ectodomain (Figure 6G), suggesting alteration in their binding in the context of the trimeric protein. Among monoclonal antibodies affected in their binding to the B.1.351 RBD (gray sector in Figure 6E), maintenance of

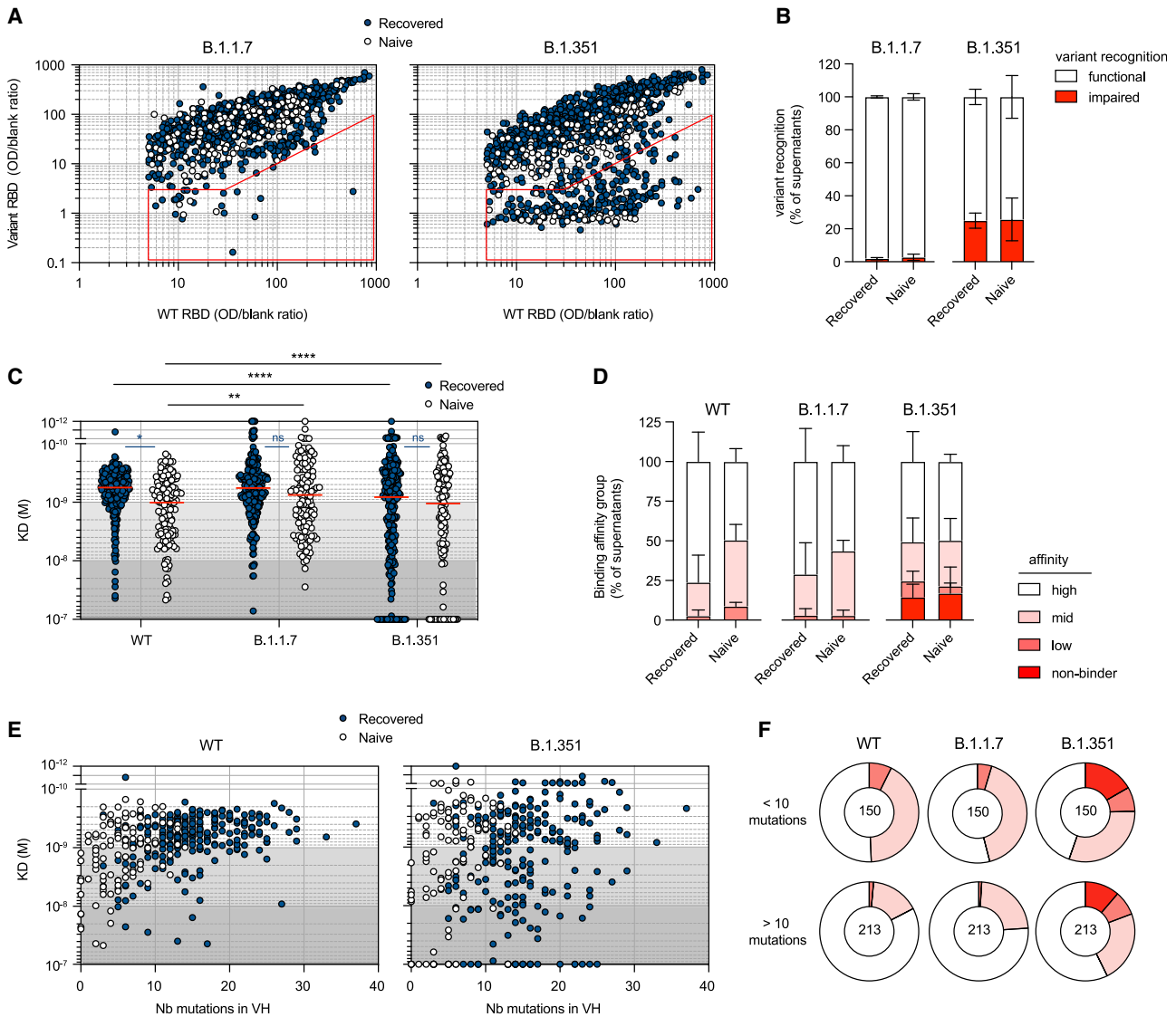


Figure 4. The MBC pool of vaccinated individuals contains high-affinity clones against WT SARS-CoV-2 and B.1.1.7 and B.1.351 VOCs

(A) WT RBD versus B.1.1.7 RBD (left) or B.1.351 RBD ELISA values (right) for all single-cell culture supernatants of RBD-specific MBCs isolated from SARS-CoV-2-recovered (dark blue, $n = 952$) and naive (white, $n = 373$) donors. Only supernatants with WT ELISA OD/blank ratio ≥ 5 are displayed. The red sector identifies naturally expressed antibodies defined as impaired in the recognition of a given variant (variant ELISA OD/blank ratio < 3 or ≥ 10 -fold decrease in variant recognition).

(B) Frequencies of single RBD-specific MBC culture supernatants with functional or impaired recognition of B.1.1.7 or B.1.351 RBD variants as assessed by ELISA.

(C) Dissociation constants (K_D , expressed as moles/L) measured by BLI for 382 naturally expressed monoclonal antibodies against WT, B.1.1.7, and B.1.351 RBD. Tested monoclonal antibodies were selected randomly from single-cell culture supernatants of RBD-specific MBCs isolated from SARS-CoV-2-recovered ($n = 251$) and naive donors ($n = 131$) and displaying WT RBD ELISA OD/blank ratio ≥ 3 . Background colors define high-affinity ($K_D < 10^{-9}$ M), mid-affinity ($10^{-9} \leq K_D < 10^{-8}$ M), and low-affinity ($10^{-8} \leq K_D < 10^{-7}$) monoclonal antibodies. All monoclonal antibodies with no measurable affinity ($K_D \geq 10^{-7}$) were considered non-binders.

(D) Histogram showing the intra-donor binding affinity distribution of monoclonal antibodies tested against WT, B.1.1.7, and B.1.351 RBD variants, as defined in (C), for SARS-CoV-2-recovered or naive donors. Bars indicate mean \pm SEM.

(E) Measured K_D (M) against WT (left) or B.1.351 RBD (right) versus number of V_H mutations for all tested monoclonal antibodies with available V_H sequence from SARS-CoV-2-recovered (dark blue, $n = 249$) and naive (white, $n = 114$) donors (Spearman correlations for all sequences: V_H mutation/WT K_D , $r = 0.3791$, $p < 0.0001$; V_H mutation/B.1.351 K_D , $r = 0.152$, $p = 0.0033$).

(F) Pie chart showing the binding affinity distribution of all tested monoclonal antibodies with low (<10 mutations, top panel) or high V_H mutation numbers (>10, bottom panel) against WT, B.1.1.7, and B.1.351 RBD variants as defined in (C). Numbers at center of the pie chart indicate the total number of tested monoclonal antibodies in each group.

A two-way ANOVA with two sets of multiple comparisons (between tested variants inside each group (black lines) and between groups for each tested variants (colored lines)) was performed (C; Benjamini, Krieger and Yekutieli FDR correction). **** $p < 0.0001$, ** $p < 0.01$, * $p < 0.05$. See also Figure S4 and Table S2.

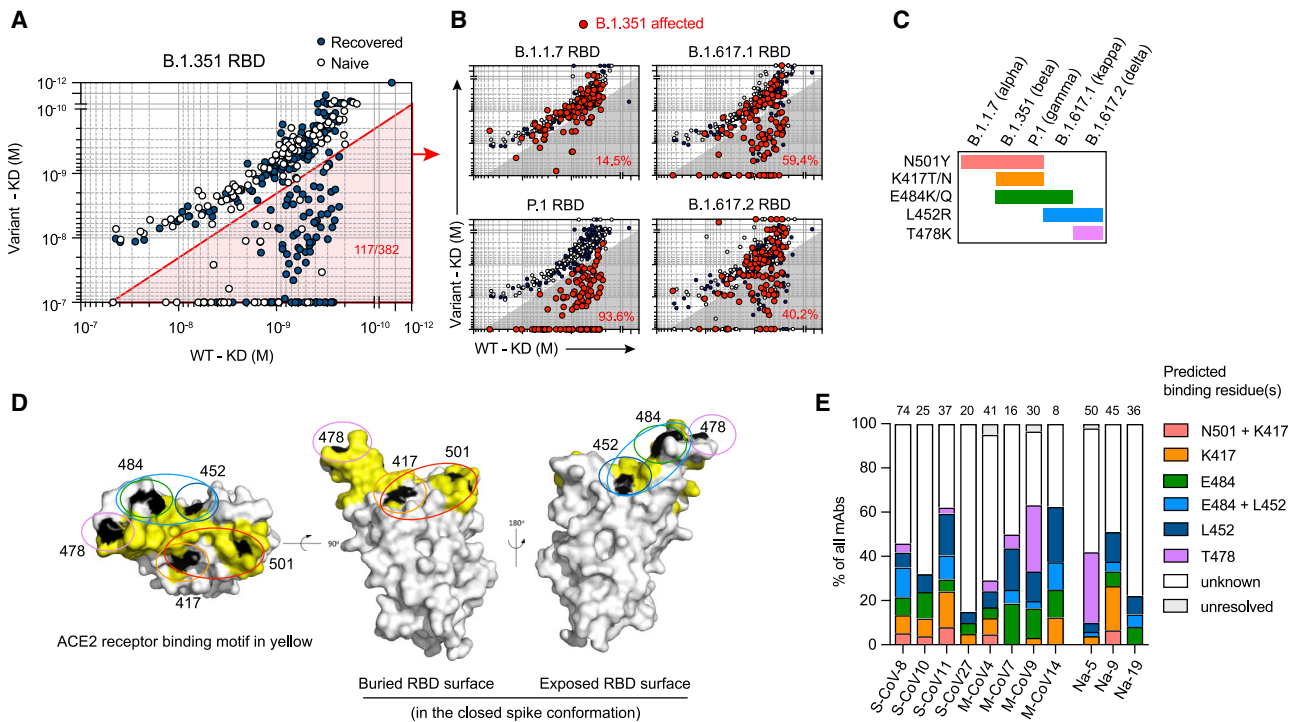


Figure 5. The variant RBD recognition profile reveals key residues recognized by MBCs mobilized by the mRNA vaccine boost

(A) Dot plot representing the K_D values for B.1.351 RBD versus WT RBD for all tested monoclonal antibodies from SARS-CoV-2-recovered (dark blue dots) and naive donors (white dots). The red shaded zone indicates B.1.351-affected monoclonal antibodies, defined as those with at least 2-fold increased K_D for B.1.351 compared with the WT RBD.

(B) Dot plots representing the K_D values for B.1.1.7, P.1, B.1.617.1, and B.1.617.2 RBD versus WT RBD. B.1.351-affected monoclonal antibodies are highlighted as larger red dots (corresponding to clones present in the red sector in A). Percentages indicate the proportion of B.1.351-affected monoclonal antibodies also affected by the indicated RBD variant.

(C) Distribution of known mutations in the RBD domain between B.1.1.7, B.1.351, P.1, B.1.617.1, and B.1.617.2 SARS-CoV-2 variants.

(D) RBD (extracted from the PDB: 6XR8 S protein trimer structure) shown in three orthogonal views, with the ACE2 receptor binding motif highlighted in yellow and the residues found mutated in at least one of the tested variants (L452, K417, T478, E484, and N501) highlighted in black. Single or a group of predicted binding residues are further highlighted by colored ovals according to the color scheme used in (E).

(E) Frequencies of predicted essential binding residues, as defined by RBD variants recognition profile in BLI, for all monoclonal antibodies isolated from each of the 11 tested donors. Numbers of tested monoclonal antibodies for each donor are indicated on top of each histogram.

See also [Figure S5](#) and [Table S2](#).

neutralization activity against the VOC was strongly dictated by their original affinity against the WT RBD. Although clones with weak initial affinity against the WT RBD were mostly impaired (red dots in the gray sector), 40% of clones with high initial affinity remained potent neutralizers against the VOC (white dots in the gray sector, [Figures 6E](#) and [6F](#)). This included monoclonals directed against the E484 and K417 residues of the SARS-CoV-2 RBD ([Figure S6C](#)). This highlights the key role of affinity maturation in shaping the humoral response and anticipating viral escape.

These results demonstrate that the MBC pool selected by the WT RBD after mRNA vaccination contains, among its diverse and affinity matured repertoire, a substantial fraction of potent neutralizers against VOCs.

DISCUSSION

MBCs display a diverse repertoire allowing an adaptive response upon re-exposure to the pathogen, especially in the case of variants ([Purtha et al., 2011](#); [Weisel et al., 2016](#)). However, repeated

antigenic stimulation with vaccinations or viral challenge may be deleterious, reducing the diversity of the overall response in which drifted epitopes are less well targeted ([Andrews et al., 2015](#); [Mesin et al., 2020](#)). Thus, understanding how mRNA vaccination affects the MBC pool shaped by a previous exposure to SARS-CoV-2 and to determine its capacity to neutralize variants is critical. More generally, to decipher how MBCs from naive vaccinees differ and evolve in comparison with SARS-CoV-2-recovered individuals is also of major importance in the pandemic context.

We report here a longitudinal study of SARS-CoV-2-recovered individuals followed over 1 year after their initial infection and vaccinated with the BNT162b2 mRNA vaccine. The vaccine response of SARS-CoV-2-naive individuals was analyzed in parallel. The strength of our approach is the large-scale, unbiased study of the MBC response against SARS-CoV-2 at the single-cell scale using *in vitro* activation of randomly sampled MBCs/ABCs. This allowed a deep functional analysis that included affinity assessment against the WT RBD and against 5 variants, including B.1.617.2, and determination of neutralization potency of these secreted IgG against two SARS-CoV-2 viruses without

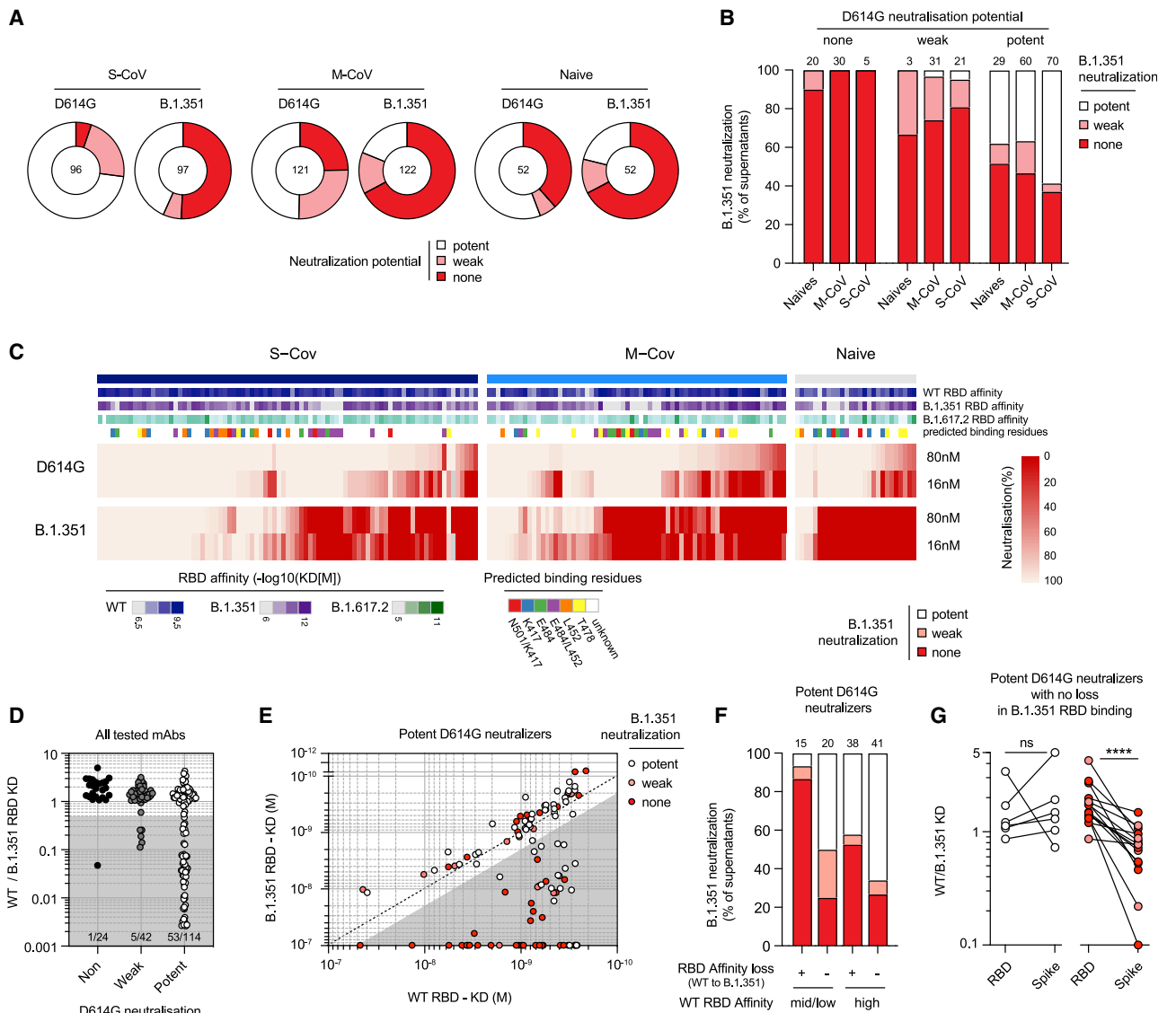


Figure 6. A substantial proportion of MBCs in vaccinated individuals neutralizes D614G SARS-CoV-2 and B.1.351 VOCs

(A) Pie charts showing the proportion of single-cell culture supernatants of RBD-specific MBCs isolated from SARS-CoV-2-recovered (S-CoV, n = 104; M-CoV, n = 123) and naive donors (n = 52) displaying potent, weak, or no neutralization potential (none) against the D614G SARS-CoV-2 and B.1.351 SARS-CoV-2 variants. Potent neutralizers are defined as more than 80% neutralization at 16 nM and weak neutralizer as neutralization less than 80% at 16 nM but more than 80% at 80 nM. Others were defined as non-neutralizing.

(B) Histogram showing the proportion of B.1.351 SARS-CoV-2 potent, weak, and non-neutralizing single-RBD-specific MBC culture supernatants, grouped based on their neutralization potency against D614G SARS-CoV-2.

(C) Heatmap showing *in vitro* neutralization of the D614G SARS-CoV-2 and B.1.351 variants at 80 nM and 16 nM for all culture supernatants whose monoclonal antibodies were also tested in BLI against all variants (S-CoV, n = 85; M-CoV, n = 67; naive, n = 27). K_D (M) values against the WT, B.1.351, and B.1.617.2 RBD for each monoclonal antibody are represented on top, along with predicted binding residues.

(D) Ratio of WT over B.1.351 RBD K_D values for all monoclonal antibodies displayed in (C), grouped based on their neutralization potency against D614G SARS-CoV-2.

(E) K_D (M) values against B.1.351 versus WT RBD for all D614G SARS-CoV-2 potent neutralizer monoclonal antibodies. Dot color indicates the neutralization potency against the B.1.351 SARS-CoV-2 variant. Gray shade highlights binding-impaired clones against the B.1.351 RBD variant as defined in Figure 5A.

(F) B.1.351 SARS-CoV-2 neutralization potency distribution of all tested potent D614G SARS-CoV-2 neutralizers, grouped based on their affinity for the WT RBD and affinity loss against B.1.351.

(G) WT versus B.1.351 variant RBD or S K_D ratio for selected monoclonal antibodies showing no clear B.1.351 RBD binding impairment and no loss (left) or clear loss (right) of neutralization potency against the B.1.351 SARS-CoV-2 variant. A paired Wilcoxon test was performed (****p < 0.0001).

See also Figure S6 and Table S2.

cloning and re-expression intermediates. We focused on the RBD because anti-RBD antibodies contribute to the majority of neutralizing antibodies, and its mutations allow immune escape of VOCs (Ju et al., 2020; Robbiani et al., 2020) together with additional targets in the N-terminal domain of the S (McCallum et al., 2021; Tong et al., 2021).

Our study highlights the stability of the overall RBD-specific MBC population up to 12 months after infection with a stable mutation profile, extending observations on memory persistence in COVID-19 (Wang et al., 2021b). The dynamics of RBD-specific cells after mRNA vaccination in SARS-CoV-2-recovered individuals reflect the plasticity of the MBC pool, which promptly and widely activates, proliferates, and generates ASCs and then contracts as resting MBCs (Goel et al., 2021a; Reynolds et al., 2021; Wang et al., 2021b). This mobilized population contains highly mutated affinity-matured clones that settle, expand, and persist for up to 2 months after the boost with a higher frequency and mutational load than before the vaccinal boost. Despite this, longitudinal VDJ sequencing revealed a limited effect on the diversity of this previously matured repertoire. Thus, expansion of the MBC pool does not seem to impair archives of the B cell specificities that have been selected during the amplification. In contrast, and mirroring early stages of the extrafollicular response after infection (Woodruff et al., 2020), RBD-specific B cells expressing near-germline recurrent V_H genes with potent affinity are recruited after mRNA vaccination in naive individuals. MBCs from naive individuals also acquired somatic mutations with time but, 2 months after the boost, harbored fewer mutations than SARS-CoV-2-recovered individuals 3 months after COVID-19. Thus, although the MBC pool matures progressively in naive vaccinees, its maturation and amplification were less pronounced, resulting in less RBD-specific MBCs compared with SARS-CoV-2-recovered individuals 12 months after infection (7.8 and 3 times less than S-CoV and M-CoV, respectively) and 2 months after the boost (18.2 and 6 times less than S-CoV and M-CoV, respectively).

As reported previously, most sera of SARS-CoV-2-recovered individuals efficiently neutralized the B.1.351 variant after the mRNA vaccine, which contrasted with the significant lower neutralization potency of the sera of naive vaccinated individuals (Goel et al., 2021a; Reynolds et al., 2021; Stamatatos et al., 2021; Wang et al., 2021b). This likely reflects the quality and maturation of the B cell pool mobilized by the vaccine; i.e., an extrafollicular response in naive vaccinees and a mature MBC response in recovered individuals.

A fraction of recurrent and convergent V_H genes of MBCs failed to recognize the B.1.351 variant RBD in both cohorts, but a large proportion of clones retained high affinity against this variant. This is consistent with a recent report showing that B cell clones expressing potent antibodies are retained selectively in the repertoire over time (Wang et al., 2021b). This phenomenon occurs independent of the mutational load, with high-affinity clones against variants present “randomly” in the MBC repertoire of SARS-CoV-2-recovered or naive individuals. So, despite the fact that the amplitude and quality of the MBC response after the mRNA vaccine appears to be lower in naive than in previously infected individuals, high-affinity clones with neutralizing potency against VOCs settle in their repertoire, suggesting that their MBC pool could compensate for the time-dependent decay of the initial antibody response.

Correlation of neutralization and affinity shows a complex profile for antibodies expressed by MBCs. Immune escape can affect high-affinity clones against the WT RBD, but, at the same time, a proportion of clones with high affinity for the WT RBD maintain neutralizing potency against B.1.351, contrasting with clones with low or weak affinity that constantly failed to neutralize variants. It indicates that high affinity provides some flexibility for antibodies to cope with mutations affecting their binding target and to conserve their neutralization potency. Consistent with a structural analysis (Yuan et al., 2021), determination of targeted epitopes using binding of different RBDs of VOCs shows that E484 preferentially affected the binding affinity of the IGHV1-2/1-69 genes and K417N and N501Y that of IGHV3-53/3-66 and IGHV1-2. It underlines that, if particular antibody lineages are affected by RBD mutations, then others may retain neutralizing properties (Barnes et al., 2020; Greaney et al., 2021a, 2021b; Muecksch et al., 2021; Scheid et al., 2021; Wang et al., 2021b).

These data describe an immune response maturing with time in SARS-CoV-2 convalescent individuals and resulting in a massive, high-affinity response after vaccination, which, even imprinted by the Wuhan-type RBD, displays improved recognition of the RBD variants as well. In this immune evolution scheme, the response of naive vaccinees nevertheless lags behind the maturation process that took place during infection. As proposed recently, vaccinated individuals will further improve the affinity and diversity of their MBC response with time and, therefore, probably also improve their quantitative and qualitative antibody response through persistence of vaccine-induced germinal centers (Cho et al., 2021; Goel et al., 2021b; Turner et al., 2021). Nonetheless, our observations in SARS-CoV-2-recovered individuals suggest that repeated challenges, even using the original S protein, will help to reduce any persisting differences and allow vaccinated people to respond more efficiently to current SARS-CoV-2 variants by recall of affinity-matured MBCs.

LIMITATIONS OF THE STUDY

The relatively small size and the limited follow-up of the cohorts do not allow us to identify characteristics of the individuals that would predict the response to the mRNA vaccine and its persistence. Furthermore, individuals with a severe form of COVID-19 were not matched for age and comorbidities with those who presented a mild form or with naive individuals; thus, differences between these groups must be interpreted with caution. Finally, we focused our study on the RBD domain of the SARS-CoV-2 S protein as it represents the major known target for neutralizing antibodies. However, neutralizing antibodies against other domains of the trimeric S have been described, notably against the N-terminal domain (NTD). Larger cohorts of individuals with a wider spectrum of age and comorbidities, extended follow-up (up to 6 months or more), and dedicated studies of non-RBD-specific neutralizing MBCs would be important in the future to provide a comprehensive picture of B cell memory responses directed against VOCs after mRNA vaccination.

STAR★METHODS

Detailed methods are provided in the online version of this paper and include the following:

- **KEY RESOURCES TABLE**
- **RESOURCE AVAILABILITY**
 - Lead contact
 - Materials availability
 - Data and code availability
- **EXPERIMENTAL MODEL AND SUBJECT DETAILS**
 - Study participants
 - Virus strains
- **METHOD DETAILS**
 - Anti-RBD (S) SARS-CoV-2 antibodies assay
 - Recombinant protein purification
 - Flow cytometry and cell sorting
 - Single-cell culture
 - ELISA
 - Single-cell IgH sequencing
 - Computational analyses of VDJ sequences
 - 3D representation of known mutations to the RBD surface
 - Affinity measurement using biolayer interferometry (Octet)
 - Virus neutralization assay
- **QUANTIFICATION AND STATISTICAL ANALYSIS**
- **ADDITIONAL RESOURCES**

SUPPLEMENTAL INFORMATION

Supplemental information can be found online at <https://doi.org/10.1016/j.immuni.2021.09.011>.

ACKNOWLEDGMENTS

We thank Garnett Kelsoe for providing the human cell culture system and invaluable advice. We thank A. Bouchartat and the Chemogenomic and Biological screening core facility headed by F. Agou as well as P. England and the Molecular Biophysics core facility at the Institut Pasteur, Paris, France for support during the course of this work. We also thank Sébastien Storck, Lucie Da Silva, and Sandra Weller for advices and support and the physicians, Constance Guillaud, Raphael Lepeule, Frédéric Schlemmer, Elena Foïs, Henri Guillet, Nicolas De Prost, and Pascal Lim, whose patients were included in this study. The graphical abstract and **Figures 1A** and **S4A** were created using BioRender. This work was initiated by a grant from the Agence Nationale de la Recherche and the Fondation pour la Recherche Médicale (ANR; MEMO-COV-2 -FRM) and funded by the Fondation Princesse Grace and by an ERC Advanced Investigator Grant (B-response). Assistance Publique – Hôpitaux de Paris (AP-HP; Département de la Recherche Clinique et du Développement) was the promotor and the sponsor of MEMO-COV-2. Work in the Unit of Structural Virology was funded by the Institut Pasteur Urgence COVID-19 Fundraising Campaign. A.S. was supported by a Poste d'Accueil from the Institut National de la Santé et de la Recherche Médicale (INSERM), I.F. by a fellowship from the Agence Nationale de Recherches sur le Sida et les Hépatites Virales (ANRS), M.B. by a CIFRE fellowship from the Association Nationale de la Recherche et de la Technologie (ANRT), and A.d.L.S. by a SNFMI fellowship. P.B. acknowledges funding from ANR (ANR-14-CE16-0011-DROPmAbs), the Institut Carnot Pasteur Microbes et Santé (ANR 11 CARN 0017-01), the Institut Pasteur, and INSERM.

AUTHOR CONTRIBUTIONS

Conceptualization, P.C., A.S., J.-C.W., C.-A.R., and M. Mahévas; data curation, P.C., A.S., M.B., G.B.-S., and I.A.; formal analysis, A.S., P.C., M.B., G.B.-S., I.A., M.B.-A., A.d.L.S., A.V., S. Fourati., and I.F.; funding acquisition, S. Fillatreau., J.-C.W., C.-A.R., and M. Mahévas; investigation, A.S., P.C., A.d.L.S., I.A., and A.V.; methodology, A.S., J.-C.W., C.-A.R., P.C., and M. Mahévas; project administration, P.C., F.C.-P., J.-C.W., C.-A.R., and M. Mahé-

vas; resources, J.-M.P., F.N.-P., S. Fourati., E.C., L.L., M. Michel, B.G., S.G., G.M., Y.N., V.Z., P.B., F.A.R., C.-A.R., and M. Mahévas; software, P.C.; supervision, P.C., J.-C.W., C.-A.R., P.B., F.R., and M. Mahévas; validation, A.S., I.A., A.V., A.d.L.S., M.B., C.-A.R., P.C., and M. Mahévas; visualization, P.C., A.S., I.A., A.d.L.S., and M. Mahévas; writing – original draft, P.C., A.S., J.-C.W., C.-A.R., and M. Mahévas; writing – review & editing, all authors.

DECLARATION OF INTERESTS

Outside of the submitted work, M. Mahévas. received research funds from GSK and personal fees from LFB and Amgen. J.-C.W. received consulting fees from Institut Mérieux. P.B. received consulting fees from Regeneron Pharmaceuticals. J.-M.P. received personal fees from Abbvie, Gilead, Merck, and Siemens Healthcare. F.R. is a member of the board of MELETIOS Therapeutics and of the Scientific Advisory Board of eureKARE.

Received: June 17, 2021

Revised: August 5, 2021

Accepted: September 14, 2021

Published: September 21, 2021

REFERENCES

- Abu-Raddad, L.J., Chemaitelly, H., and Butt, A.A.; National Study Group for COVID-19 Vaccination (2021). Effectiveness of the BNT162b2 Covid-19 Vaccine against the B.1.1.7 and B.1.351 Variants. *N. Engl. J. Med.* **385**, 187–189.
- Andrews, S.F., Huang, Y., Kaur, K., Popova, L.I., Ho, I.Y., Pauli, N.T., Henry Dunand, C.J., Taylor, W.M., Lim, S., Huang, M., et al. (2015). Immune history profoundly affects broadly protective B cell responses to influenza. *Sci. Transl. Med.* **7**, 316ra192.
- Baden, L.R., El Sahly, H.M., Essink, B., Kotloff, K., Frey, S., Novak, R., Diemert, D., Spector, S.A., Rouphael, N., Creech, C.B., et al.; COVE Study Group (2021). Efficacy and Safety of the mRNA-1273 SARS-CoV-2 Vaccine. *N. Engl. J. Med.* **384**, 403–416.
- Barnes, C.O., West, A.P., Jr., Huey-Tubman, K.E., Hoffmann, M.A.G., Sharaf, N.G., Hoffman, P.R., Koranda, N., Gristick, H.B., Gaebler, C., Muecksch, F., et al. (2020). Structures of Human Antibodies Bound to SARS-CoV-2 Spike Reveal Common Epitopes and Recurrent Features of Antibodies. *Cell* **182**, 828–842.e16.
- Cai, Y., Zhang, J., Xiao, T., Peng, H., Sterling, S.M., Walsh, R.M., Jr., Rawson, S., Rits-Volloch, S., and Chen, B. (2020). Distinct conformational states of SARS-CoV-2 spike protein. *Science* **369**, 1586–1592.
- Cele, S., Gazy, I., Jackson, L., Hwa, S.-H., Tegally, H., Lustig, G., Giandhari, J., Pillay, S., Wilkinson, E., Naidoo, Y., et al.; Network for Genomic Surveillance in South Africa; COMMIT-KZN Team (2021). Escape of SARS-CoV-2 501Y.V2 from neutralization by convalescent plasma. *Nature* **593**, 142–146.
- Cherian, S., Potdar, V., Jadhav, S., Yadav, P., Gupta, N., Das, M., Das, S., Agarwal, A., Singh, S., Abraham, P., et al. (2021). Convergent evolution of SARS-CoV-2 spike mutations, L452R, E484Q and P681R, in the second wave of COVID-19 in Maharashtra, India. *bioRxiv*. <https://doi.org/10.1101/2021.04.22.440932>.
- Cho, A., Muecksch, F., Schaefer-Babajew, D., Wang, Z., Finkin, S., Gaebler, C., Ramos, V., Cipolla, M., Agudelo, M., Bednarski, E., et al. (2021). Antibody Evolution after SARS-CoV-2 mRNA Vaccination. *bioRxiv*. <https://doi.org/10.1101/2021.07.29.454333>.
- Crickx, E., Chappert, P., Sokal, A., Weller, S., Azzaoui, I., Vandenberghe, A., Bonnard, G., Rossi, G., Fadeev, T., Storck, S., et al. (2021). Rituximab-resistant splenic memory B cells and newly engaged naive B cells fuel relapses in patients with immune thrombocytopenia. *Sci. Transl. Med.* **13**, eabc3961.
- Dagan, N., Barda, N., Kepten, E., Miron, O., Perchik, S., Katz, M.A., Hernán, M.A., Lipsitch, M., Reis, B., and Balicer, R.D. (2021). BNT162b2 mRNA Covid-19 Vaccine in a Nationwide Mass Vaccination Setting. *N. Engl. J. Med.* **384**, 1412–1423.
- Davies, N.G., Abbott, S., Barnard, R.C., Jarvis, C.I., Kucharski, A.J., Munday, J.D., Pearson, C.A.B., Russell, T.W., Tully, D.C., Washburne, A.D., et al.;

- CMMID COVID-19 Working Group; COVID-19 Genomics UK (COG-UK) Consortium (2021). Estimated transmissibility and impact of SARS-CoV-2 lineage B.1.1.7 in England. *Science* 372, eabg3055.
- Dugan, H.L., Stamper, C.T., Li, L., Changrob, S., Asby, N.W., Halfmann, P.J., Zheng, N.-Y., Huang, M., Shaw, D.G., Cobb, M.S., et al. (2021). Profiling B cell immunodominance after SARS-CoV-2 infection reveals antibody evolution to non-neutralizing viral targets. *Immunity* 54, 1290–1303.e7.
- Ebinger, J.E., Fert-Bober, J., Printsev, I., Wu, M., Sun, N., Prostko, J.C., Frias, E.C., Stewart, J.L., Van Eyk, J.E., Braun, J.G., et al. (2021). Antibody responses to the BNT162b2 mRNA vaccine in individuals previously infected with SARS-CoV-2. *Nat. Med.* 27, 981–984.
- Edara, V.V., Norwood, C., Floyd, K., Lai, L., Davis-Gardner, M.E., Hudson, W.H., Mantus, G., Nyhoff, L.E., Adelman, M.W., Fineman, R., et al. (2021). Infection- and vaccine-induced antibody binding and neutralization of the B.1.351 SARS-CoV-2 variant. *Cell Host Microbe* 29, 516–521.e3.
- Ellebedy, A.H., Jackson, K.J.L., Kissick, H.T., Nakaya, H.I., Davis, C.W., Roskin, K.M., McElroy, A.K., Oshansky, C.M., Elbein, R., Thomas, S., et al. (2016). Defining antigen-specific plasmablast and memory B cell subsets in human blood after viral infection or vaccination. *Nat Immunol.* 17, 1226–1234.
- Gaebler, C., Wang, Z., Lorenzi, J.C.C., Muecksch, F., Finkin, S., Tokuyama, M., Cho, A., Jankovic, M., Schaefer-Babajew, D., Oliveira, T.Y., et al. (2021). Evolution of antibody immunity to SARS-CoV-2. *Nature* 597, 639–644.
- Garcia-Beltran, W.F., Lam, E.C., St Denis, K., Nitido, A.D., Garcia, Z.H., Hauser, B.M., Feldman, J., Pavlovic, M.N., Gregory, D.J., Poznansky, M.C., et al. (2021). Multiple SARS-CoV-2 variants escape neutralization by vaccine-induced humoral immunity. *Cell* 184, 2372–2383.e9.
- Goel, R.R., Apostolidis, S.A., Painter, M.M., Mathew, D., Pattekar, A., Kuthuru, O., Gouma, S., Hicks, P., Meng, W., Rosenfeld, A.M., et al. (2021a). Distinct antibody and memory B cell responses in SARS-CoV-2 naïve and recovered individuals following mRNA vaccination. *Sci. Immunol.* 6, eabi6950.
- Goel, R.R., Painter, M.M., Apostolidis, S.A., Mathew, D., Meng, W., Rosenfeld, A.M., Lundgreen, K.A., Reynaldi, A., Khoury, D.S., Pattekar, A., et al. (2021b). mRNA Vaccination Induces Durable Immune Memory to SARS-CoV-2 with Continued Evolution to Variants of Concern. *bioRxiv*. <https://doi.org/10.1101/2021.08.23.457229>.
- Greaney, A.J., Loes, A.N., Crawford, K.H.D., Starr, T.N., Malone, K.D., Chu, H.Y., and Bloom, J.D. (2021a). Comprehensive mapping of mutations in the SARS-CoV-2 receptor-binding domain that affect recognition by polyclonal human plasma antibodies. *Cell Host Microbe* 29, 463–476.e6.
- Greaney, A.J., Starr, T.N., Barnes, C.O., Weisblum, Y., Schmidt, F., Caskey, M., Gaebler, C., Cho, A., Agudelo, M., Finkin, S., et al. (2021b). Mapping mutations to the SARS-CoV-2 RBD that escape binding by different classes of antibodies. *Nat. Commun.* 12, 4196.
- Gupta, N.T., Vander Heiden, J.A., Uduman, M., Gadala-Maria, D., Yaari, G., and Kleinstein, S.H. (2015). Change-O: a toolkit for analyzing large-scale B cell immunoglobulin repertoire sequencing data. *Bioinformatics* 31, 3356–3358.
- Hacisuleyman, E., Hale, C., Saito, Y., Blachere, N.E., Bergh, M., Conlon, E.G., Schaefer-Babajew, D.J., DaSilva, J., Muecksch, F., Gaebler, C., et al. (2021). Vaccine Breakthrough Infections with SARS-CoV-2 Variants. *N. Engl. J. Med.* 384, 2212–2218.
- Harvey, W.T., Carabelli, A.M., Jackson, B., Gupta, R.K., Thomson, E.C., Harrison, E.M., Ludden, C., Reeve, R., Rambaut, A., Peacock, S.J., and Robertson, D.L.; COVID-19 Genomics UK (COG-UK) Consortium (2021). SARS-CoV-2 variants, spike mutations and immune escape. *Nat. Rev. Microbiol.* 19, 409–424.
- Hoffmann, M., Arora, P., Groß, R., Seidel, A., Hörnich, B.F., Hahn, A.S., Krüger, N., Graichen, L., Hofmann-Winkler, H., Kempf, A., et al. (2021). SARS-CoV-2 variants B.1.351 and P.1 escape from neutralizing antibodies. *Cell* 184, 2384–2393.e12.
- Hsieh, C.-L., Goldsmith, J.A., Schaub, J.M., DiVenere, A.M., Kuo, H.-C., Javanmardi, K., Le, K.C., Wrapp, D., Lee, A.G., Liu, Y., et al. (2020). Structure-based design of prefusion-stabilized SARS-CoV-2 spikes. *Science* 369, 1501–1505.
- Ju, B., Zhang, Q., Ge, J., Wang, R., Sun, J., Ge, X., Yu, J., Shan, S., Zhou, B., Song, S., et al. (2020). Human neutralizing antibodies elicited by SARS-CoV-2 infection. *Nature* 584, 115–119.
- Konstantinidis, T.G., Zisaki, S., Mitroulis, I., Konstantinidou, E., Kontekaki, E.G., Romanidou, G., Karvelas, A., Nanousi, I., Lazidis, L., Cassimos, D., et al. (2021). Levels of Produced Antibodies after Vaccination with mRNA Vaccine; Effect of Previous Infection with SARS-CoV-2. *J. Clin. Med.* 10, 2842.
- Krammer, F., Srivastava, K., Alshammery, H., Amoako, A.A., Awawda, M.H., Beach, K.F., Bermúdez-González, M.C., Bielak, D.A., Carreño, J.M., Chernet, R.L., et al. (2021). Antibody Responses in Seropositive Persons after a Single Dose of SARS-CoV-2 mRNA Vaccine. *N. Engl. J. Med.* 384, 1372–1374.
- Lad, L., Clancy, S., Kovalenko, M., Liu, C., Hui, T., Smith, V., and Pragatis, N. (2015). High-throughput kinetic screening of hybridomas to identify high-affinity antibodies using bio-layer interferometry. *J. Biomol. Screen.* 20, 498–507.
- Luo, X.M., Maarschalk, E., O'Connell, R.M., Wang, P., Yang, L., and Baltimore, D. (2009). Engineering human hematopoietic stem/progenitor cells to produce a broadly neutralizing anti-HIV antibody after in vitro maturation to human B lymphocytes. *Blood* 113, 1422–1431.
- Manisty, C., Otter, A.D., Treibel, T.A., McKnight, Á., Altmann, D.M., Brooks, T., Noursadeghi, M., Boyton, R.J., Semper, A., and Moon, J.C. (2021). Antibody response to first BNT162b2 dose in previously SARS-CoV-2-infected individuals. *Lancet* 397, 1057–1058.
- McCallum, M., De Marco, A., Lempp, F.A., Tortorici, M.A., Pinto, D., Walls, A.C., Beltramello, M., Chen, A., Liu, Z., Zatta, F., et al. (2021). N-terminal domain antigenic mapping reveals a site of vulnerability for SARS-CoV-2. *Cell* 184, 2332–2347.e16.
- Mesin, L., Schiepers, A., Ersching, J., Barbulescu, A., Cavazzoni, C.B., Angelini, A., Okada, T., Kurosaki, T., and Victoria, G.D. (2020). Restricted Clonality and Limited Germinal Center Reentry Characterize Memory B Cell Reactivation by Boosting. *Cell* 180, 92–106.e11.
- Muecksch, F., Weisblum, Y., Barnes, C.O., Schmidt, F., Schaefer-Babajew, D., Lorenzi, J.C.C., Flyak, A.I., DeLaitch, A.T., Huey-Tubman, K.E., Hou, S., et al. (2021). Affinity maturation of SARS-CoV-2 neutralizing antibodies confers potency, breadth, and resilience to viral escape mutations. *Immunity* 54, 1853–1868.e7.
- Planas, D., Bruel, T., Grzelak, L., Guivel-Benhassine, F., Staropoli, I., Porrot, F., Planchais, C., Buchrieser, J., Rajah, M.M., Bishop, E., et al. (2021a). Sensitivity of infectious SARS-CoV-2 B.1.1.7 and B.1.351 variants to neutralizing antibodies. *Nat. Med.* 27, 917–924.
- Planas, D., Veyer, D., Baidaliuk, A., Staropoli, I., Guivel-Benhassine, F., Rajah, M.M., Planchais, C., Porrot, F., Robillard, N., Puech, J., et al. (2021b). Reduced sensitivity of SARS-CoV-2 variant Delta to antibody neutralization. *Nature* 596, 276–280.
- Plante, J.A., Liu, Y., Liu, J., Xia, H., Johnson, B.A., Lokugamage, K.G., Zhang, X., Muruato, A.E., Zou, J., Fontes-Garfias, C.R., et al. (2021). Spike mutation D614G alters SARS-CoV-2 fitness. *Nature* 592, 116–121.
- Polack, F.P., Thomas, S.J., Kitchin, N., Absalon, J., Gurtman, A., Lockhart, S., Perez, J.L., Pérez Marc, G., Moreira, E.D., Zerbini, C., et al.; C4591001 Clinical Trial Group (2020). Safety and Efficacy of the BNT162b2 mRNA Covid-19 Vaccine. *N. Engl. J. Med.* 383, 2603–2615.
- Purtha, W.E., Tedder, T.F., Johnson, S., Bhattacharya, D., and Diamond, M.S. (2011). Memory B cells, but not long-lived plasma cells, possess antigen specificities for viral escape mutants. *J. Exp. Med.* 208, 2599–2606.
- Reynolds, C.J., Pade, C., Gibbons, J.M., Butler, D.K., Otter, A.D., Menacho, K., Fontana, M., Smit, A., Sackville-West, J.E., Cutino-Moguel, T., et al.; UK COVIDsortium Immune Correlates Network; UK COVIDsortium Investigators (2021). Prior SARS-CoV-2 infection rescues B and T cell responses to variants after first vaccine dose. *Science*, eabh1282.
- Robbiani, D.F., Gaebler, C., Muecksch, F., Lorenzi, J.C.C., Wang, Z., Cho, A., Agudelo, M., Barnes, C.O., Gazumyan, A., Finkin, S., et al. (2020). Convergent antibody responses to SARS-CoV-2 in convalescent individuals. *Nature* 584, 437–442.

- Rodda, L.B., Netland, J., Shehata, L., Pruner, K.B., Morawski, P.A., Thouvenel, C.D., Takehara, K.K., Eggenberger, J., Hemann, E.A., Waterman, H.R., et al. (2021). Functional SARS-CoV-2-Specific Immune Memory Persists after Mild COVID-19. *Cell* 184, 169–183.e17.
- Saadat, S., Rikhtegaran Tehrani, Z., Logue, J., Newman, M., Frieman, M.B., Harris, A.D., and Sajadi, M.M. (2021). Binding and Neutralization Antibody Titers After a Single Vaccine Dose in Health Care Workers Previously Infected With SARS-CoV-2. *JAMA* 325, 1467–1469.
- Sakharkar, M., Rappazzo, C.G., Wieland-Alter, W.F., Hsieh, C.-L., Wrapp, D., Esterman, E.S., Kaku, C.I., Wec, A.Z., Geoghegan, J.C., McLellan, J.S., et al. (2021). Prolonged evolution of the human B cell response to SARS-CoV-2 infection. *Sci. Immunol.* 6, eabg6916.
- Samanovic, M.I., Cornelius, A.R., Wilson, J.P., Karmacharya, T., Gray-Gaillard, S.L., Allen, J.R., Hyman, S.W., Moritz, G., Ali, M., Korolov, S.B., et al. (2021). Poor antigen-specific responses to the second BNT162b2 mRNA vaccine dose in SARS-CoV-2-experienced individuals. *medRxiv*. <https://doi.org/10.1101/2021.02.07.21251311>.
- Scheid, J.F., Barnes, C.O., Eraslan, B., Hudak, A., Keeffe, J.R., Cosimi, L.A., Brown, E.M., Muecksch, F., Weisblum, Y., Zhang, S., et al. (2021). B cell genomics behind cross-neutralization of SARS-CoV-2 variants and SARS-CoV. *Cell* 184, 3205–3221.e24.
- Sokal, A., Chappert, P., Barba-Spaeth, G., Roeser, A., Fourati, S., Azaoui, I., Vandenberghe, A., Fernandez, I., Meola, A., Bouvier-Alias, M., et al. (2021). Maturation and persistence of the anti-SARS-CoV-2 memory B cell response. *Cell* 184, 1201–1213.e14.
- Stamatatos, L., Czartoski, J., Wan, Y.-H., Homad, L.J., Rubin, V., Glantz, H., Neradilek, M., Seydoux, E., Jennewein, M.F., MacCamy, A.J., et al. (2021). mRNA vaccination boosts cross-variant neutralizing antibodies elicited by SARS-CoV-2 infection. *Science*, eabg9175.
- Starr, T.N., Greaney, A.J., Dingens, A.S., and Bloom, J.D. (2021). Complete map of SARS-CoV-2 RBD mutations that escape the monoclonal antibody LY-CoV555 and its cocktail with LY-CoV016. *Cell Rep Med* 2, 100255.
- Supasa, P., Zhou, D., Dejnirattisai, W., Liu, C., Mentzer, A.J., Ginn, H.M., Zhao, Y., Duyvesteyn, H.M.E., Nutalai, R., Tuekprakhon, A., et al. (2021). Reduced neutralization of SARS-CoV-2 B.1.1.7 variant by convalescent and vaccine sera. *Cell* 184, 2201–2211.e7.
- Tegally, H., Wilkinson, E., Giovanetti, M., Iranzadeh, A., Fonseca, V., Giandhari, J., Doolabh, D., Pillay, S., San, E.J., Msomi, N., et al. (2021). Detection of a SARS-CoV-2 variant of concern in South Africa. *Nature* 592, 438–443.
- Tiller, T., Meffre, E., Yurasov, S., Tsuiji, M., Nussenzweig, M.C., and Wardemann, H. (2008). Efficient generation of monoclonal antibodies from single human B cells by single cell RT-PCR and expression vector cloning. *J. Immunol. Methods* 329, 112–124.
- Tong, P., Gautam, A., Windsor, I.W., Travers, M., Chen, Y., Garcia, N., Whiteman, N.B., McKay, L.G.A., Storm, N., Malsick, L.E., et al. (2021). Memory B cell repertoire for recognition of evolving SARS-CoV-2 spike. *Cell* 184, 4969–4980.
- Turner, J.S., O'Halloran, J.A., Kalaidina, E., Kim, W., Schmitz, A.J., Zhou, J.Q., Lei, T., Thapa, M., Chen, R.E., Case, J.B., et al. (2021). SARS-CoV-2 mRNA vaccines induce persistent human germinal centre responses. *Nature* 596, 109–113.
- Wang, P., Nair, M.S., Liu, L., Iketani, S., Luo, Y., Guo, Y., Wang, M., Yu, J., Zhang, B., Kwong, P.D., et al. (2021a). Antibody resistance of SARS-CoV-2 variants B.1.351 and B.1.1.7. *Nature* 593, 130–135.
- Wang, Z., Muecksch, F., Schaefer-Babajew, D., Finkin, S., Viant, C., Gaebler, C., Hoffmann, H.-H., Barnes, C.O., Cipolla, M., Ramos, V., et al. (2021b). Naturally enhanced neutralizing breadth against SARS-CoV-2 one year after infection. *Nature* 595, 426–431.
- Weisel, F.J., Zuccarino-Catania, G.V., Chikina, M., and Shlomchik, M.J. (2016). A Temporal Switch in the Germinal Center Determines Differential Output of Memory B and Plasma Cells. *Immunity* 44, 116–130.
- Weissman, D., Alameh, M.-G., de Silva, T., Collini, P., Hornsby, H., Brown, R., LaBranche, C.C., Edwards, R.J., Sutherland, L., Santra, S., et al. (2021). D614G Spike Mutation Increases SARS CoV-2 Susceptibility to Neutralization. *Cell Host Microbe* 29, 23–31.e4.
- Woodruff, M.C., Ramonell, R.P., Nguyen, D.C., Cashman, K.S., Saini, A.S., Haddad, N.S., Ley, A.M., Kyu, S., Howell, J.C., Ozturk, T., et al. (2020). Extrafollicular B cell responses correlate with neutralizing antibodies and morbidity in COVID-19. *Nat. Immunol.* 21, 1506–1516.
- Xie, X., Liu, Y., Liu, J., Zhang, X., Zou, J., Fontes-Garfias, C.R., Xia, H., Swanson, K.A., Cutler, M., Cooper, D., et al. (2021). Neutralization of SARS-CoV-2 spike 69/70 deletion, E484K and N501Y variants by BNT162b2 vaccine-elicited sera. *Nat. Med.* 27, 620–621.
- Yuan, M., Huang, D., Lee, C.D., Wu, N.C., Jackson, A.M., Zhu, X., Liu, H., Peng, L., van Gils, M.J., Sanders, R.W., et al. (2021). Structural and functional ramifications of antigenic drift in recent SARS-CoV-2 variants. *Science* 373, 818–823.
- Yurkovetskiy, L., Wang, X., Pascal, K.E., Tomkins-Tinch, C., Nyallie, T.P., Wang, Y., Baum, A., Diehl, W.E., Dauphin, A., Carbone, C., et al. (2020). Structural and Functional Analysis of the D614G SARS-CoV-2 Spike Protein Variant. *Cell* 183, 739–751.e8.

STAR★METHODS

KEY RESOURCES TABLE

REAGENT or RESOURCE	SOURCE	IDENTIFIER
Antibodies		
CD3	Biologend	Clone: UCHT1; Cat#300425; RRID: AB_830754
CD14	BD Bioscience	Clone: M φP9; Cat#561709; RRID: AB_1645464
CD19	BD Bioscience	Clone: HIB19; Cat# 562321; RRID: AB_11154408
CD38	BD Bioscience	Clone: HIT2; Cat# 551400; RRID AB_394184
CD27	Biologend	Clone: M-T271; Cat# 356417; RRID: AB_2562598
CD11c	BD Bioscience	Clone: S-HCL-3; Cat#744436; RRID: AB_2742232
IgD	Life technologies	Clone: Polyclonal; Cat# H15501; RRID: AB_2536563
His Tag	Biologend	Clone: J095G46; Cat# 362605; RRID:AB_2563634
His Tag	Biologend	Clone: J095G46; Cat# 362603; RRID:AB_2715818
CD71	Biologend	Clone: CY1G4; Cat# 334111; RRID:AB_2563118
CD21	BD Bioscience	Clone: B-ly4; Cat#563163 ; RRID:AB_2741028
N SARS-CoV-2	Institut Pasteur	Rabbit polyclonal (N.Escriou)
Anti-Human Fc Capture Biosensors	Sartorius	Cat#18-5060
Biological samples		
Cryopreserved PBMCs from S-Cov, M-Cov and naive patients	Henri Mondor Hospital, Assistance Publique des Hôpitaux de Paris	N/A
D614G SARS-CoV-2 virus (hCoV-19/France/GE1973/2020)	Institut Pasteur, CNR Respiratory Viruses (S.Van der Werf)	N/A
B.1.351 SARS-CoV-2 virus (CNR 202100078)	Institut Pasteur, CNR Respiratory Viruses (S.Van der Werf)	N/A
B.1.617.2 SARS-CoV-2 virus (2021/17.2 200 (GISAID ID: EPI_ISL_2029113))	Institut Pasteur, Virus and Immunity Unit (O. Schwartz)	N/A
Chemical, peptides, and recombinant proteins		
SARS-CoV-2 Spike	Institut Pasteur, Virologie Structurale (F. Rey)	N/A
B.1.351 SARS-CoV-2 Spike	Institut Pasteur, Virologie Structurale (F. Rey)	N/A
WT SARS-CoV-2 RBD	Institut Pasteur, Virologie Structurale (F. Rey)	N/A
B.1.1.7 SARS-CoV-2 RBD	Institut Pasteur, Virologie Structurale (F. Rey)	N/A
B.1.351 SARS-CoV-2 RBD	Institut Pasteur, Virologie Structurale (F. Rey)	N/A
P.1 SARS-CoV-2 RBD	Institut Pasteur, Virologie Structurale (F. Rey)	N/A
B.1.617.1 SARS-CoV-2 RBD	Institut Pasteur, Virologie Structurale (F. Rey)	N/A
B.1.617.2 SARS-CoV-2 RBD	Institut Pasteur, Virologie Structurale (F. Rey)	N/A
Live dead aqua	Life technologies,	Cat#L34957
Recombinant human IL-2	PeproTech	Cat#200-02
Recombinant human IL-4	PeproTech	Cat#200-04
Recombinant human IL-21	PeproTech	Cat#210-21
Recombinant human BAFF	PeproTech	Cat#310-13
Software and algorithms		
Kaluza v2.1	Beckman Coulter	https://www.beckman.fr
Flowjo v10.7.1	FlowJo, LLC	https://www.flowjo.com
GraphPad Prism v9	GraphPad	https://www.graphpad.com
Codon Code Aligner v9	Codon Code Corporation	https://www.codoncode.com/
R v4.0.2	R Foundation	https://www.r-project.org
RStudio v1.3.1056	RStudio	https://rstudio.com
IgBLASTn v1.16.0	NCBI	https://www.ncbi.nlm.nih.gov/igblast/

(Continued on next page)

Continued

REAGENT or RESOURCE	SOURCE	IDENTIFIER
HT Data analysis software 11.1	ForteBio	https://www.sartorius.com
Adobe Illustrator (CS6)	Adobe	https://www.adobe.com
PyMOL Molecular Graphics System, v2.1	Schrödinger, LLC	https://pymol.org/

RESOURCE AVAILABILITY**Lead contact**

Further information and requests for resources and reagents should be directed to and will be fulfilled by the Lead Contact, Matthieu Mahévas (matthieu.mahevas@aphp.fr).

Materials availability

No unique materials were generated for this study.

Data and code availability

- Single cell culture VDJ sequencing data reported in [Figure 3](#) and [Figure S3](#) are directly included in this study as part of [Table S3](#).
- This paper does not report original code.
- Any additional information required to reanalyze the data reported in this paper is available from the lead contact upon request.

EXPERIMENTAL MODEL AND SUBJECT DETAILS**Study participants**

In total, 43 patients with recovered COVID-19 (17 S-CoV and 26 M-CoV) and 25 naive patients were included in this study and sampled at least one time before boost vaccination (12 months post infection for recovered or after the prime for naive) or after boost vaccination (boost + 7 days or boost + 2 months). Among the 43 SARS-CoV-2 recovered patients, 34 were from the original MEMO-COV-2 cohort and followed up to 12 months post-infection and/or vaccination. Seventeen of these patients had severe COVID-19 (patients requiring oxygen, S-CoV) and 17 had a mild COVID-19 disease (mainly healthcare workers, M-CoV). An additional cohort of 9 patients who also experienced mild COVID-19 during the first wave of pandemic in France and were vaccinated at least six months after the infection were specifically recruited for this study. SARS-CoV-2 infection was defined as confirmed reverse transcriptase polymerase chain reaction (RT-PCR) on nasal swab or clinical presentation associated with typical aspect on CT-scan and/or serological evidence. Twenty-five healthcare workers who had no history of COVID-19 and negative IgG anti-nucleocapsid (and/or Spike) were enrolled in the naive group (IRB 2018-A01610-55). Detailed information on the individuals, including gender and health status, can be found in [Table S1](#).

All vaccinated subjects received the BNT162b2 mRNA vaccine. SARS-CoV-2 recovered patients received only one dose, in line with French guidelines, except 3 who received 2 doses (See [Table S1](#)). First injection was realized in mean 309 days (\pm SD 44.6 days) after the infection. Naive patients received two doses at a mean 27.7 days (\pm SD 1.8 days) interval.

Prior to vaccination, samples were collected from SARS-CoV-2 recovered patients 12 months post symptoms onset (mean \pm SD: 329.1 \pm 15.8 days after disease onset for S-CoV, and 342.0 \pm 8.6 days after disease onset for M-CoV). Samples at 12 months post disease onset were defined as “pre-boost.” For patients not sampled before vaccination ($n = 9/34$), sample at 6 months was considered as “pre-boost.” For SARS-CoV-2 naive patients, the “prime” time-point was defined as the sampling between the two doses and was drawn at a mean 20.2 \pm 5.9 days after the first injection.

Samples were additionally collected shortly after the boost (mean \pm SD: 10 \pm 5.3 days for S-CoV; 23 \pm 6.1 days for M-CoV and 9 \pm 4.0 days for naive), and 2 months after the boost (mean \pm SD: 64.7 \pm 15.3 days for S-CoV ; 63.2 \pm 11.9 days for M-CoV and 63.3 \pm 9.0 days for naive). Clinical and biological characteristics of these patients are summarized in [Table S1](#). Patients were recruited at the Henri Mondor University Hospital (AP-HP), between March and April 2021. MEMO-COV-2 study (NCT04402892) was approved by the ethical committee Ile-de-France VI (Number: 40-20 HPS), and was performed in accordance with the French law. Written informed consent was obtained from all participants.

Virus strains

The reference D614G strain (hCoV-19/France/GE1973/2020) and the B.1.351 strain (CNR 202100078) were supplied by the National Reference Centre for Respiratory Viruses hosted by Institut Pasteur and headed by Sylvie van der Werf. The B.1.617.2 SARS-CoV-2-variant Delta/2021/17.2 200 (GISAID ID: EPI_ISL_2029113) was supplied by the Virus and Immunity Unit hosted by Institut Pasteur (Paris, France) and headed by Olivier Schwartz ([Planas et al., 2021b](#)). The viral strains were supplied through the European Virus Archive goes Global (EVAg) platform, a project that has received funding from the European Union’s Horizon 2020 research and innovation program under grant agreement number 653316.

D614G, B.1.351, and B.1.617.2 viral stocks were prepared by amplification and titration in Vero E6 cells and were used at passage 3 and passage 2 respectively. Single use aliquots stored at -80°C were used for all the assays.

METHOD DETAILS

Anti-RBD (S) SARS-CoV-2 antibodies assay

Serum samples were analyzed for anti-S-RBD IgG titers with the SARS-CoV-2 IgG Quant II assay (ARCHITECT[®], Abbott Laboratories). The latter assay is an automated chemiluminescence microparticle immunoassay (CMIA) that quantifies anti-RBD IgG, with 50 AU/mL as a positive cut-off and a maximal threshold of quantification of 40,000 AU/mL. All assays were performed by trained laboratory technicians according to the manufacturer's standard procedures.

Recombinant protein purification

Construct design

The ectodomain from the SARS-CoV-2 Spike (residues 1-1208) was designed as a stabilized construct with six proline mutations (F817P, A892P, A899P, A942P, K986P, V987P), a GSAS substitution at the furin cleavage site (residues 682-685) and a C-terminal Foldon trimerization motif (Hsieh et al., 2020), followed by Hisx8, Strep and Avi tags. This construct was cloned using its endogenous signal peptide in pcDNA3.1(+).

The SARS-CoV-2 Receptor Binding Domain (RBD) was cloned in pcDNA3.1(+) encompassing the Spike (S) residues 331-528, and it was flanked by an N-terminal IgK signal peptide and a C-terminal Thrombin cleavage site followed by Hisx8, Strep and Avi tags. The mutations present on the B.1.1.7 (N501Y), B.1.351 (K417N, E484K, N501Y), P.1 (K417T, E484K, N501Y), B.1.617.1 (L452R, E484Q) and B.1.617.2 (L452R, T478K) variants were introduced by PCR mutagenesis using standard methods.

Protein expression and purification

Plasmids coding for recombinant proteins were transiently transfected in Expi293FTM cells (Thermo Fischer) using FectoPRO[®] DNA transfection reagent (Polyplus), according to the manufacturer's instructions. Cells were incubated at 37°C for 5 days and then the culture was centrifuged and the supernatant was concentrated. Proteins were purified from the supernatant by affinity chromatography using StrepTactin columns (IBA) (SARS-CoV-2 S) or His-TrapTM Excel columns (Cytiva) (SARS-CoV-2 RBD). A final step of size-exclusion chromatography (SEC) in PBS was also performed, using either a Superose6 10/300 column (Cytiva) for the SARS-CoV-2 S, or a Superdex200 10/300 (Cytiva) for the SARS-CoV-2 RBD.

Flow cytometry and cell sorting

PBMCs were isolated from venous blood samples via standard density gradient centrifugation and used after cryopreservation at -150°C . Cells were thawed in RPMI-1640 (GIBCO)-10% FBS (GIBCO), washed twice and incubated with 5 μg of the SARS-CoV-2 His-tagged spike protein or WT RBD in 100 μL of PBS (GIBCO)-2% FBS during 20 min on ice. For each condition, 2.5×10^6 cells were washed and resuspended in the same conditions, then the fluorochrome-conjugated antibody cocktail including the 2 anti-His antibodies was added at pre-titrated concentrations (1:100 for CD19, CD21, CD11c, CD71, CD38, CD3, CD14 and IgD, 1:50 for CD27 and 1:33 for anti-His tag) for 20 min at 4°C and viable cells were identified using a LIVE/DEAD Fixable Aqua Dead Cell Stain Kit (Thermo Fisher Scientific, 1:200) incubated with conjugated antibodies. Samples were acquired using a LSR Fortessa SORP (BD Biosciences). For cell sorting, cells were stained using the same protocol and then sorted in 96 plates using the ultra-purity mode on a MA900 cell sorter (SONY), or Aria III (BD Biosciences). Data were analyzed with FlowJo or Kaluza softwares. Detailed gating strategies for individual markers are depicted in [Figure S2A](#).

For Uniform Manifold Approximation and Projection (UMAP) generation and visualization ([Figure 2](#)), FCS files from 5 S-CoV, 8 M-CoV and 4 naive patients with complete panel acquisition at pre boost, boost + 7 days and boost + 2 months ([Table S1](#)) were concatenated. The UMAP (v3.1) plugin in FlowJO was used to calculate the UMAP coordinates for the resulting 536.161 cells (with 30 neighbors, metric = euclidian and minimum distance = 0.5 as default parameters). The FlowSOM (v2.6) plugin was used in parallel on the same downsampled dataset to create a self-organizing map (using $n = 10$ clusters as default parameter). This self-organizing map was then applied to the initial FCS files to calculate both total and RBD-specific MBC repartition in identified clusters on all collected cells for each donor. Naive patients were not further analyzed due to the very low number of RBD specific B cells. Both UMAP and FlowSOM plugin were run on viable dump⁺ CD19⁺ IgD⁻ cells taking into account fluorescent intensities from the following parameters: FSC-A, SSC-A, CD19, CD21, CD11c, CD71, CD38, CD27 and IgD, while excluding the dump (CD3 and CD14), viability and RBD channels. Contour plots (equal probability contouring, with intervals set to 5% of gated populations) for each identified cluster were further overlaid on UMAP projection in FlowJO. For visualization purposes, only the outermost density representing 95% of the total gated cells was kept for the final figure, all other contour lines were removed in Adobe Illustrator.

Single-cell culture

Single cell culture was performed as previously described ([Crickx et al., 2021](#)). Single B cells were sorted in 96-well plates containing MS40L^{lo} cells expressing CD40L (kind gift from G. Kelsoe; [Luo et al., 2009](#)). Cells were co-cultured at 37°C with 5% CO₂ during 21 or 25 days in RPMI-1640 (Invitrogen) supplemented with 10% HyClone FBS (Thermo Scientific), 55 μM 2-mercaptoethanol, 10 mM HEPES, 1 mM sodium pyruvate, 100 units/mL penicillin, 100 $\mu\text{g}/\text{mL}$ streptomycin, and MEM non-essential amino acids (all Invitrogen), with the addition of recombinant human BAFF (10 ng/ml), IL2 (50 ng/ml), IL4 (10 ng/ml), and IL21 (10 ng/ml; all Peprotech). Part

of the supernatant was carefully removed at days 4, 8, 12, 15 and 18 and the same amount of fresh medium with cytokines was added to the cultures. After 21 days of single cell culture, supernatants were harvested and stored at -20°C . Cell pellets were placed on ice and gently washed with PBS (GIBCO) before being resuspended in $50\ \mu\text{L}$ of RLT buffer (QIAGEN) supplemented with 1% 2-mercaptoethanol and subsequently stored at -80°C until further processing.

ELISA

Total IgG and SARS-CoV-2 WT RBD, B.1.1.7 RBD and B.1.351 RBD-specific IgG from culture supernatants were measured using homemade ELISA. 96 well ELISA plates (Thermo Fisher) were coated with either goat anti-human Ig ($10\ \mu\text{g}/\text{ml}$, Invitrogen) or recombinant SARS-CoV-2 WT RBD, B.1.1.7 RBD or B.1.351 RBD protein ($2.5\ \mu\text{g}/\text{ml}$ each) in sodium carbonate during 1h at 37°C . After plate blocking, cell culture supernatants were added for 1hr, then ELISA were developed using HRP-goat anti-human IgG ($1\ \mu\text{g}/\text{ml}$, Immunotech) and TMB substrate (Eurobio). OD450 and OD620 were measured and Ab-reactivity was calculated after subtraction of blank wells. Supernatants whose ratio of OD450-OD620 over control wells (consisting of supernatant from wells that contained spike-negative MBCs from the same single cell culture assay) was over 3 were considered as positive for WT RBD, B.1.1.7 RBD or B.1.351 RBD ELISA. PBS was used to define background OD450-OD620.

Single-cell IgH sequencing

Clones whose culture had proven successful (IgG concentration $\geq 1\ \mu\text{g}/\text{mL}$ at day 21-25) were selected and extracted using the NucleoSpin96 RNA extraction kit (Macherey-Nagel) according to the manufacturer's instructions. A reverse transcription step was then performed using the SuperScript IV enzyme (ThermoFisher) in a $14\ \mu\text{L}$ final volume (42°C 10 min, 25°C 10 min, 50°C 60 min, 94°C 5 min) with $4\ \mu\text{L}$ of RNA and random hexamers (ThermoFisher scientific). A PCR was further performed based on the protocol established by Tiller et al. (2008). Briefly, $3.5\ \mu\text{L}$ of cDNA was used as template and amplified in a total volume of $40\ \mu\text{L}$ with a mix of forward L-VH primers (Table S3) and reverse C γ primer and using the HotStar[®] Taq DNA polymerase (QIAGEN) and 50 cycles of PCR (94°C 30 s, 58°C 30 s, 72°C 60 s). PCR products were sequenced with the reverse primer CHG-D1 and read on ABI PRISM 3130XL genetic analyzer (Applied Biosystems). Sequence quality was verified using CodonCode Aligner software (CodonCode Corporation).

For specific patients and time points (see Table S1), some IgH sequences were obtained directly from single-cell sorting in $4\ \mu\text{L}$ lysis buffer containing PBS (GIBCO), DTT (ThermoFisher) and RNasin (Promega). Reverse transcription and a first PCR was performed as described above (50 cycles) before a second 50-cycles PCR using 5' Agel VH primer mix and C γ -CH1 3' primer, before sequencing.

Computational analyses of VDJ sequences

Processed FASTA sequences from cultured single-cell V_H sequencing were annotated using Igbblast v1.16.0 against the human IMGT reference database. Clonal cluster assignment (DefineClones.py) and germline reconstruction (CreateGermlines.py) were performed using the Immcantation/Change-O toolkit (Gupta et al., 2015) on all heavy chain V sequences. Sequences that had the same V-gene, same J-gene, including ambiguous assignments, and same CDR3 length with maximal length-normalized nucleotide hamming distance of 0.15 were considered as belonging to the same clonal group. Mutation frequencies in V genes were then calculated using the calcObservedMutations() function from the Immcantation/SHazaM v1.0.2 R package. V_H repartitions and Shannon entropies were calculated using the countGenes() and alphaDiversity() functions from the Immcantation/alakazam v1.1.0 R package. Further clonal analyses on all productively rearranged sequences were implemented in R. Graphics were obtained using the ggplot2 v3.3.3, pheatmap v1.0.12 and circlize v0.4.12 packages.

3D representation of known mutations to the RBD surface

Figure 5D was prepared with The PyMOL Molecular Graphics System, Version 2.1 Schrödinger, LLC. The atomic model used for the RBD was extracted from the cryo-EM structure of the SARS-CoV-2 spike trimer (PDB:6XR8; Cai et al., 2020)

Affinity measurement using biolayer interferometry (Octet)

This high-throughput kinetic screening of supernatants using single antigen concentration has recently been extensively tested and demonstrated excellent correlation with multiple antigen concentration measurements (Lad et al., 2015). Biolayer interferometry assays were performed using the Octet HTX instrument (ForteBio). Anti-Human Fc Capture (AHC) biosensors (18-5060) were immersed in supernatants from single-cell MBC cultures (or control monoclonal antibody) at 25°C for 1800 s. Biosensors were equilibrated for 10 minutes in 10x PBS buffer with surfactant Tween 20 (Xantec B PBST10-500) diluted 1x in sterile water with 0.1% BSA added (PBS-BT) prior to measurement. Association was performed for 600 s in PBS-BT with WT or variant RBD at 100nM followed by dissociation for 600 s in PBS-BT. Biosensor regeneration was performed by alternating 30 s cycles of regeneration buffer (glycine HCl, 10 mM, pH 2.0) and 30 s of PBS-BT for 3 cycles. Traces were reference sensor subtracted and curve fitting was performed using a local 1:1 binding model in the HT Data analysis software 11.1 (ForteBio). Sensors with response values (maximum RBD association) below 0.1nm were considered non-binding. WT RBD non-binding monoclonal antibodies ($n = 14/414$) were excluded from further analysis. For variant RBD non-binding mAbs, sensor-associated data (mAb loading and response) were manually checked to ensure that this was not the result of poor mAb loading. Following the final tested RBD variant (B.1.617.2), 18 sensors were excluded due to mAb loading issues, leaving 382 mAb included in the final analysis. For binding clones, only those with full $R^2 > 0.8$ were retained for KD reporting (Figure 4 and Figure S4) and initial prediction of key binding residues. mAbs were defined as affected against a given variant RBD if the ratio of calculated KD value against that RBD variant and the WT RBD was superior to two. Key binding residues

prediction was simply made based on mutations repartition in the different variants (Figure 5C); for example mAbs affected only by B.1.351 and P.1 variants were predicted to bind to the K417 residue. Two exceptions to these simple rules were made: 1/ mAbs affected by the B.1.1.7, B.1.351 and P.1 variants were initially labeled as binding to the N501 residue but the ratios of KD values against the B.1.351 and P.1 RBD variants and the B.1.1.7 RBD variants were further calculated. All mAbs with ratio superior to two for these two combinations were labeled as binding both the N501 and K417 residues, as previously described for RBS-A type of anti-RBD mAbs (Yuan et al., 2021); 2/ mAbs affected by the B.1.351, P.1, B.1.617.1 and B.1.617.2 variants, but not the B.1.1.7 variant, were labeled as binding both the E484 and L452 residues based on reported data in the literature for RBS-B/C antibodies (Yuan et al., 2021; Starr et al., 2021). Sensors with missing values were manually inspected to resolve binding residues attribution, leaving only four with an unresolved profile. This analysis was further confirmed by conserved intra-clonal residue binding as illustrated in Table S2H.

Virus neutralization assay

Virus neutralization was evaluated by a focus reduction neutralization test (FRNT). Vero E6 cells were seeded at 2×10^4 cells/well in a 96-well plate 24h before the assay. Two-hundred focus-forming units (ffu) of each virus were pre-incubated with serial dilutions of heat-inactivated sera or B cell clone supernatants for 1hr at 37°C before infection of cells for 2hrs. The virus/antibody mix was then removed and foci were left to develop in presence of 1.5% methylcellulose for 2 days. Cells were fixed with 4% formaldehyde and foci were revealed using a rabbit anti-SARS-CoV-2 N antibody (gift of Nicolas Escriou) and anti-rabbit secondary HRP-conjugated secondary antibody. Foci were visualized by diaminobenzidine (DAB) staining and counted using an Immunospot S6 Analyzer (Cellular Technology Limited CTL). B cell culture media and supernatants from RBD negative clones were used as negative control. Pre-pandemic serum (March 2012) was used as negative control for sera titration and was obtained from an anonymous donor through the ICAReB platform (BRIF code n°BB-0033-00062) of Institut Pasteur that collects and manages bioresources following ISO (International Organization for Standardization) 9001 and NF S 96-900 quality standards.

Percentage of virus neutralization was calculated as $(100 - ((\#foci\ sample / \#foci\ control) * 100))$. Sera IC_{50} were calculated over 6 four-fold serial dilutions from 1/10 to 1/10000 using the equation $\log(\text{inhibitor})$ versus normalized response – Variable slope in Prism 9 (GraphPad software LLC). For some of the sera (namely SARS-CoV-2 recovered post-boost), we were not able to obtain a complete neutralization curve and set up an arbitrary IC_{50} cut off of $> 1/2560$ sera dilution. For culture supernatants, two IgG concentrations (80 nM and 16 nM) were tested for each sample and each virus. Potent neutralizers were defined as $> 80\%$ neutralization at 16 nM, weak neutralizer as neutralization $< 80\%$ at 16 nM but $> 80\%$ at 80 nM. Others were defined as non-neutralizing.

QUANTIFICATION AND STATISTICAL ANALYSIS

Ordinary One-way ANOVA, Two-way ANOVA, Repeated-measures mixed effects model analysis, Kruskal-Wallis test and Mann-Whitney test were used to compare continuous variables as appropriate (indicated in Figures). Benjamini, Krieger and Yekutieli FDR correction was used for all multiple comparisons. A P -value ≤ 0.05 was considered statistically significant. Statistical analyses were all performed using GraphPad Prism 9.0 (La Jolla, CA, USA).

ADDITIONAL RESOURCES

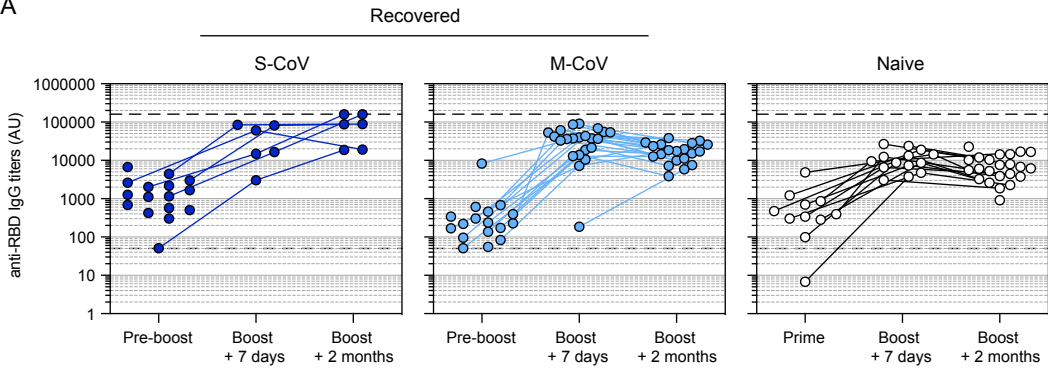
ClinicalTrials.gov Identifier: MEMO-CoV2, NCT04402892.

Supplemental information

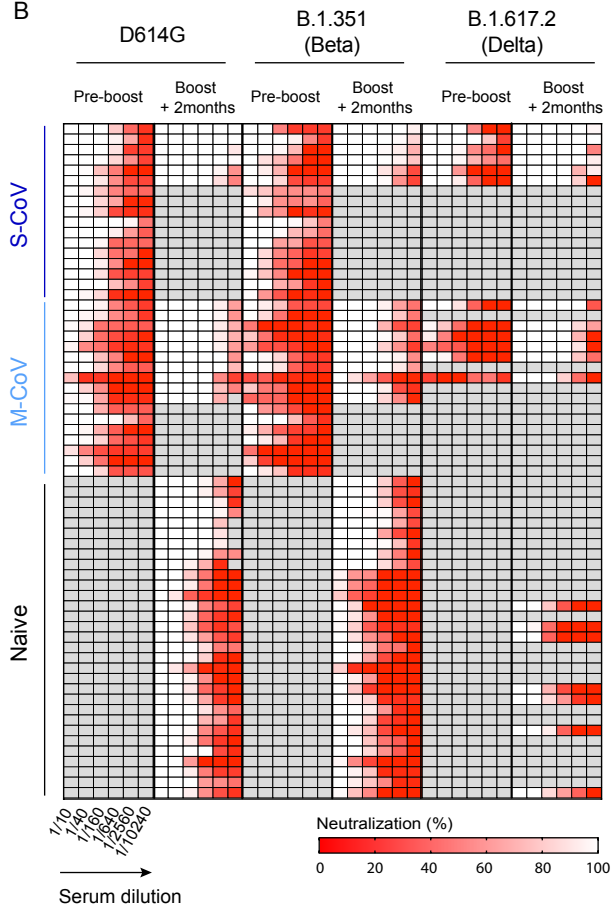
**mRNA vaccination of naive and COVID-19-recovered
individuals elicits potent memory B cells
that recognize SARS-CoV-2 variants**

Aurélien Sokal, Giovanna Barba-Spaeth, Ignacio Fernández, Matteo Broketa, Imane Azzaoui, Andréa de La Selle, Alexis Vandenberghe, Slim Fourati, Anais Roeser, Annalisa Meola, Magali Bouvier-Alias, Etienne Crickx, Laetitia Languille, Marc Michel, Bertrand Godeau, Sébastien Gallien, Giovanna Melica, Yann Nguyen, Virginie Zarrouk, Florence Canoui-Poitaine, France Pirene, Jérôme Mégret, Jean-Michel Pawlotsky, Simon Fillatreau, Pierre Bruhns, Felix A. Rey, Jean-Claude Weill, Claude-Agnès Reynaud, Pascal Chappert, and Matthieu Mahévas

A



B



C

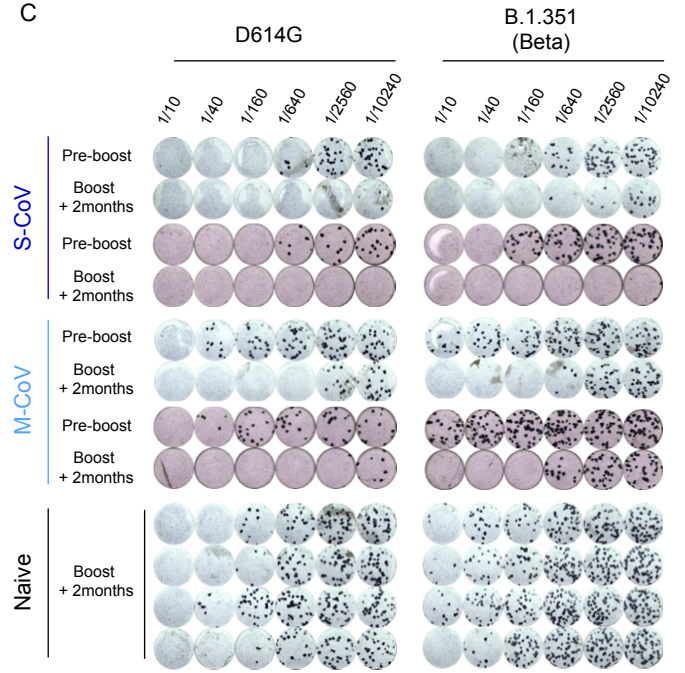


Figure S1. mRNA vaccination boosts humoral response against WT SARS-CoV-2 and VOCs in naive and SARS-CoV-2 recovered patients. Related to Figure 1.

(A) Evolution of the anti-SARS-CoV-2 RBD serum IgG titers after BNT162b2 vaccination for each patient. ELISA values are shown at pre-boost (M6 or M12) for SARS-CoV-2 recovered (S-CoV: dark blue; left panel and M-CoV: light blue, middle panel) or after the prime for naive patients (white, right panel), as well as 7 days and 2 months after the vaccine boost. **(B)** Heatmap representing the observed in vitro neutralization of D614G SARS-CoV-2 (left), B.1.351 (middle) and B.1.617.2 (right) VOCs by sera from SARS-CoV-2 recovered and naive donors at the pre-boost and boost + 2 months time points (serial dilutions: 1/10, 1/40, 1/160, 1/640, 1/2560, 1/10240). Each line represents one patient tested against SARS-CoV-2. **(C)** Representative wells for the in vitro neutralization assay of sera against D641G SARS-CoV-2 (left) and B.1.351 VOC (right). Dark blue spots represent SARS-CoV-2 infected cells.

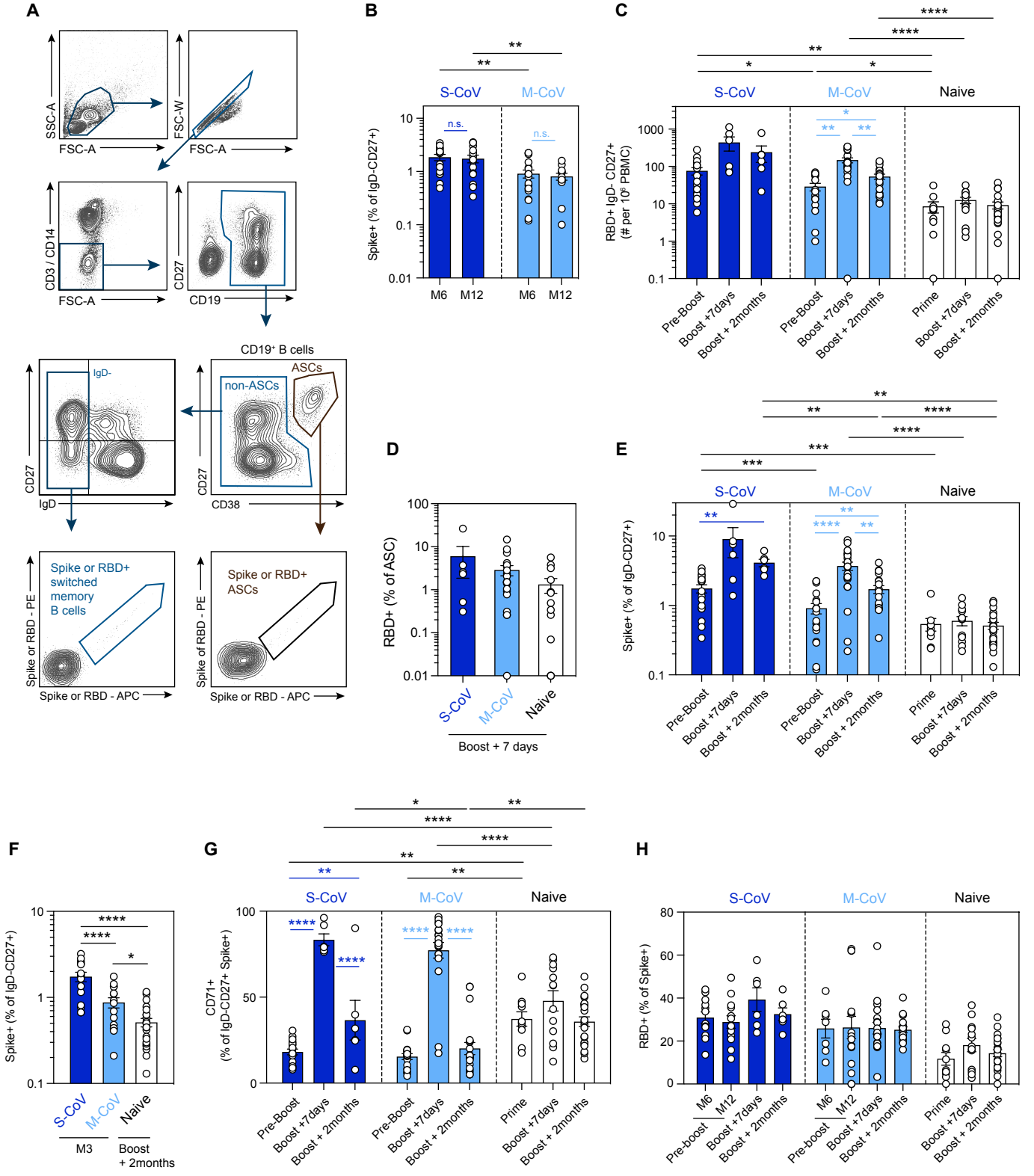


Figure S2. mRNA vaccination mobilizes SARS-CoV-2 Spike-specific B cells in SARS-CoV-2 recovered and naive patients. Related to Figure 2.

(A) Flow cytometric gating strategy for the analysis and sorting of SARS-CoV-2 S or RBD-specific MBCs or ASCs from PBMCs of SARS-CoV-2 recovered and naive donors. Lymphocytes were first gated based on morphology, before exclusion of doublets, dead cells and CD3/CD14 cells. CD19⁺ cells were then gated and subdivided into CD38^{int/-} cells (non-ASCs) and CD27⁺CD38^{hi} plasma cells (ASCs). CD38^{int/-} B cells were further divided in four quadrants using CD27 and IgD staining. Upper left quadrant defines MBCs, lower left quadrant double-negative (DN), upper right quadrant CD27⁺IgD⁺ cells (MZB) and lower right quadrant naive B cells. SARS-Cov-2 S or RBD-specific B cells were then analyzed within the B cell population of interest using a His-tagged SARS-Cov-2 S or RBD protein further revealed by two fluorescently labeled anti-His antibodies, ASCs at this stage keeping their surface BCR expression. **(B)** Frequencies of SARS-CoV-2 S-specific cells in live CD19⁺IgD⁻CD27⁺CD38^{int/-} MBCs at 6 (M6) and 12 months (M12) post symptom onset in SARS-CoV-2 recovered patients (S-CoV; dark blue, n=17/14; M-CoV: light blue, n=16/12). **(C)** Absolute numbers of RBD-specific IgD⁻CD27⁺ MBCs at pre-boost, boost + 7 days and boost + 2 months time points in S-CoV (dark blue, n=17/6/6), M-CoV (light-blue, n=14/21/20) and naive (white, n=10/13/23) patients. **(D)** Frequencies of RBD-specific cells in live ASCs at boost + 7 days in SARS-CoV-2 recovered patients (S-CoV; dark blue, n=6; M-CoV: light blue, n=21) and naive (white, n=13) donors. **(E-F)** Frequencies of SARS-CoV-2 S-specific cells in live CD19⁺IgD⁻CD27⁺CD38^{int/-} MBCs at pre-boost, boost + 7 days and boost + 2 months time points in SARS-CoV-2 recovered patients (S-CoV; dark blue, n=17/6/6; M-CoV: light blue, n=14/21/20) and naive (white, n=10/13/23) (E) and at 3 months post symptoms onset in SARS-CoV-2 recovered compared to naive individuals at the boost + 2 months time point (3 months after the prime) (F). **(G)** Frequencies of SARS-CoV-2 S-specific cells displaying an activated B cell (CD19⁺CD27⁺IgD⁻CD71⁺) phenotype at pre-boost, boost + 7 days and boost + 2 months time points in SARS-CoV-2 recovered patients (S-CoV; dark blue, n=17/6/6; M-CoV: light blue, n=14/21/20) and naive (white, n=10/13/23) donors. Bars indicate mean ±SEM. **(H)** Proportion of Spike-specific MBCs recognizing RBD in each individual at 6 months and 12 months in SARS-CoV-2

recovered and prime in naïve, and its evolution 7 days and 2 months after the boost. Bars indicate mean \pm SEM. (B) two-way ANOVA with multiple comparisons of all groups means; (C and E-G) Repeated measures mixed effects model analysis with two sets of multiple comparisons (between donor groups inside each time-point (black lines) and between time points for each donor group (colored lines)) and (D) ordinary one-way ANOVA were performed (Benjamini, Krieger and Yekutieli FDR correction was used for all multiple comparisons). Only significant comparisons are highlighted in panels (C-F). (**** $P < 0.0001$, *** $P < 0.001$, ** $P < 0.01$, * $P < 0.05$)

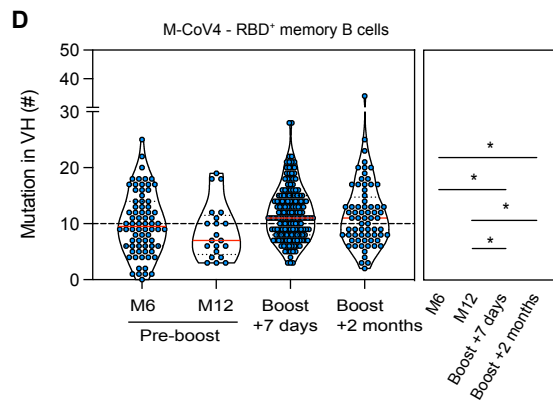
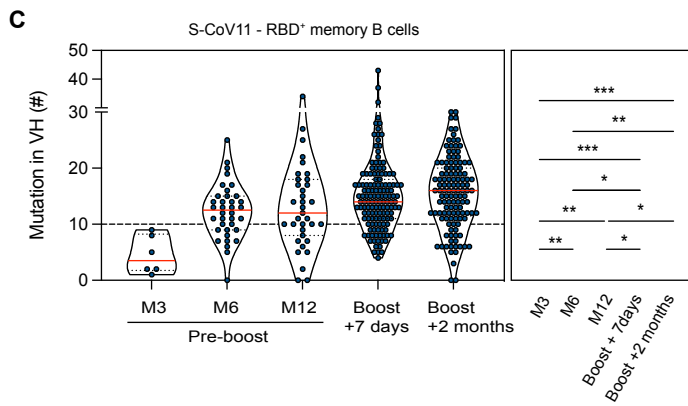
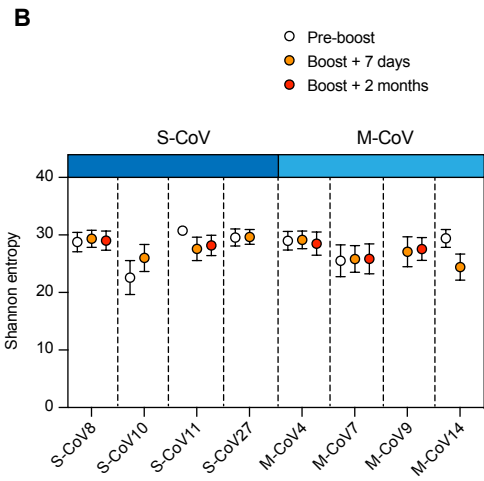
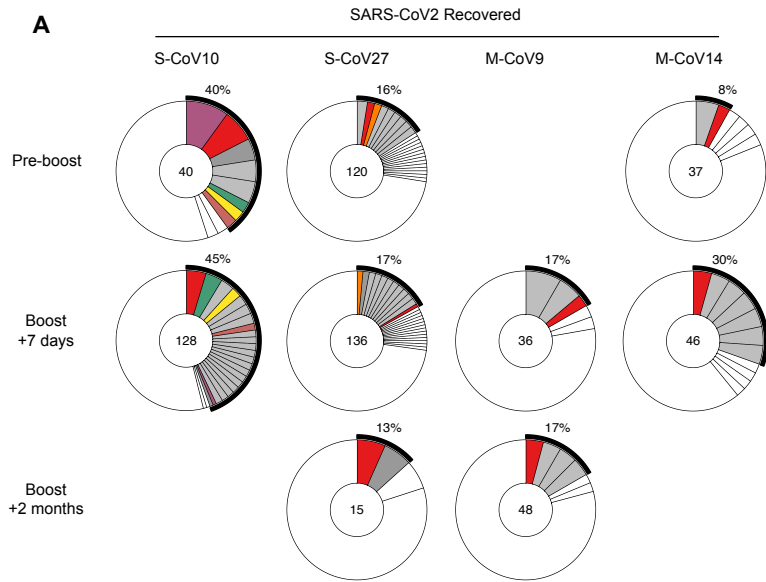


Figure S3. mRNA vaccination elicits a diverse RBD-specific memory B cell repertoire with increased mutational load in SARS-CoV-2 recovered patients. Related to Figure 3.

(A) Pie charts representing the clonal distribution of RBD-specific MBCs sorted from 2 S-CoV and 2 M-CoV at pre-boost, boost + 7 days and boost + 2 months time points. Colored slices indicate an expanded MBC clone (2 or more sequences at a given time-point) found at several time points in the same patient (persistent), grey slices indicate an expanded MBC clone found at a single time-point and white slices indicate persistent unique sequences. Outer black semi circular line indicates the proportion of sequences belonging to expanded clones at a given time point. Total number of sequences is indicated in the middle of the pie. (B) Shannon entropy index at indicated time points for the 4 S-CoV and the 4 M-CoV patients from Figure 3B and S3A. Estimated diversity \pm SD. (C-D) Violin plots showing the longitudinal evolution of the number of mutations in V_H genes of sorted RBD⁺ MBCs in one S-CoV (C) and one M-CoV donor (D). Red lines indicate median. Ordinary one-way ANOVA with multiple comparisons (Benjamini, Krieger and Yekutieli FDR correction) (***) $P < 0.001$, ** $P < 0.01$, * $P < 0.05$).

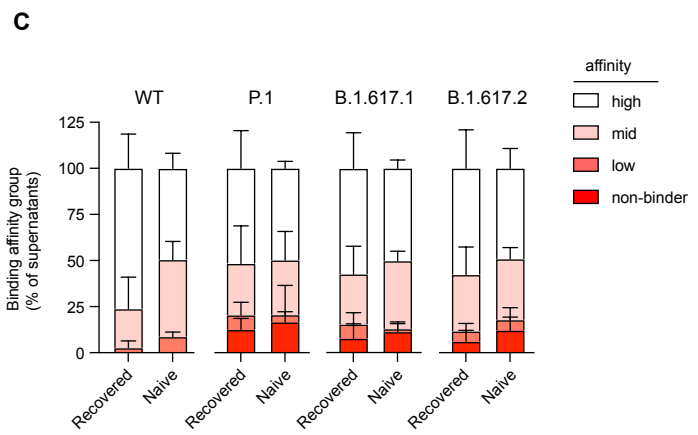
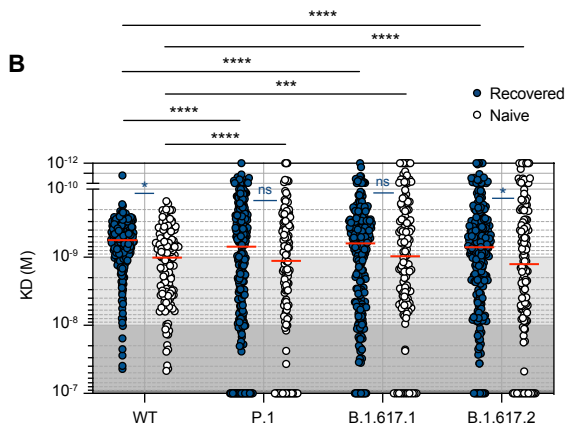
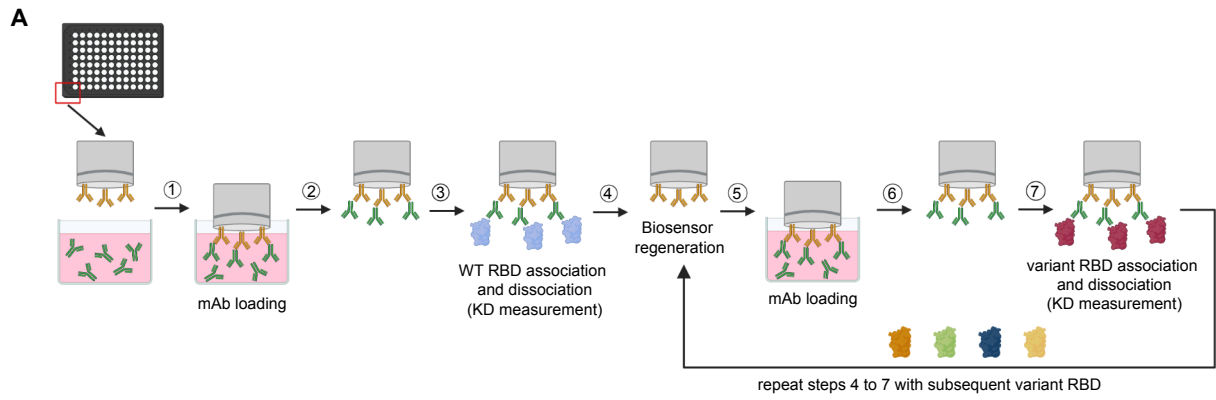


Figure S4. The memory B cell pool of vaccinated individuals contains high-affinity clones against WT SARS-CoV-2 and P.1, B.1.617.1 and B.1.617.2 VOCs. Related to Figure 4.

(A) Scheme of the experimental procedure of affinity measurement from single-cell culture supernatants against SARS-CoV-2 variant RBD using bio-layer interferometry (BLI). Monoclonal antibodies in a given supernatant were captured on an anti-human Fc coated biosensor and affinity was first measured against the WT RBD. The biosensors were then regenerated, re-loaded with the same supernatant before testing affinity against another RBD variant. This procedure was repeated to test a total of five variants (B.1.1.7; B.1.351; P.1; B.1.617.1 and B.1.617.2). (B) KD (M) measured by BLI for 382 naturally expressed monoclonal antibodies analyzed in Figure 4 and tested here against WT, P.1, B.1.617.1 and B.1.617.2 RBD variants. Tested monoclonal antibodies were randomly selected from single-cell culture supernatants of RBD-specific MBCs isolated from SARS-CoV-2 recovered (n=251) and naive donors (n=131) and displaying WT RBD ELISA blank ratio ≥ 3 . Background colors define high ($KD < 10^{-9}$ M), mid ($10^{-9} \leq KD < 10^{-8}$ M) and low ($10^{-8} \leq KD < 10^{-7}$) affinity monoclonal antibodies. All monoclonal antibodies with no measurable affinity ($KD \geq 10^{-7}$) were considered non-binders. (C) Histogram showing binding affinity distribution of tested monoclonal antibodies against WT, P.1, B.1.617.1 and B.1.617.2 RBD variants, as defined in (A), for SARS-CoV-2 recovered or naive donors. Bars indicate mean \pm SEM. (A) A two-way ANOVA with two sets of multiple comparisons (between tested variants inside each group (black lines) and between groups for each tested variants (colored lines) was performed (Benjamini, Krieger and Yekutieli FDR correction) (** $P < 0.001$; **** $P < 0.0001$).

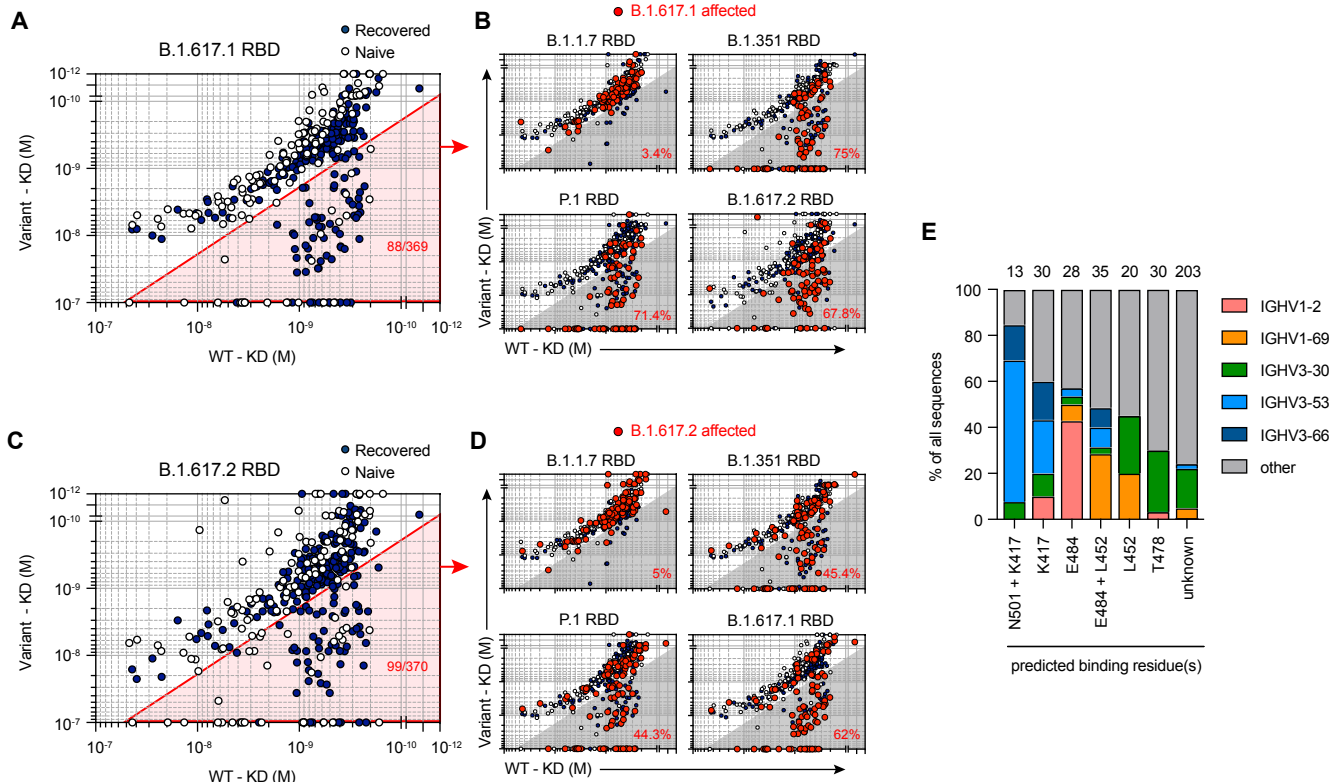


Figure S5: Variant RBD recognition profile reveals key residues recognized by memory B cells mobilized by the mRNA vaccine boost. Related to Figure 5.

(A) Dot plots representing the KDs for B.1.617.1 RBD versus WT RBD for all tested monoclonal antibodies from SARS-CoV-2 recovered (dark blue dots) and naive donors (white dots). The red shaded zone indicates B.1.617.1-affected monoclonal antibodies, defined as those whose KD for B.1.617.1 is increased by at least two-fold as compared to WT RBD. **(B)** Dot plots representing the KDs for B.1.1.7, B.1.351, P.1 and B.1.617.2 RBD versus WT RBD. B.1.617.1-affected monoclonal antibodies are highlighted as larger size red dots (corresponding to the red sector in (A)). Percentages indicate the proportion of B.1.617.1 affected monoclonal antibodies also affected by other RBD variants. **(C)** Dot plots representing the KDs for B.1.617.2 RBD versus WT RBD for all tested monoclonal antibodies from SARS-CoV-2 recovered (dark blue dots) and naive donors (white dots). The red shaded zone indicates B.1.617.2 affected monoclonal antibodies, defined as those whose KD for B.1.617.2 is increased by at least two-fold as compared to WT RBD. **(D)** Dot plots representing the KDs for B.1.1.7, B.1.351, P.1 and B.1.617.1 RBD versus WT RBD. B.1.617.2-affected monoclonal antibodies are highlighted as larger size red dots (corresponding to the red sector in (C)). Percentages indicate the proportion of B.1.617.2 affected monoclonal antibodies also affected by other RBD variants. **(E)** Proportion of IGHV1-2, IGHV1-69, IGHV3-30, IGHV3-53 and IGHV3-66 usage among all tested monoclonal antibodies with available V_H sequence and grouped based on their predicted essential binding residues, as defined by RBD variant recognition profile in BLI.

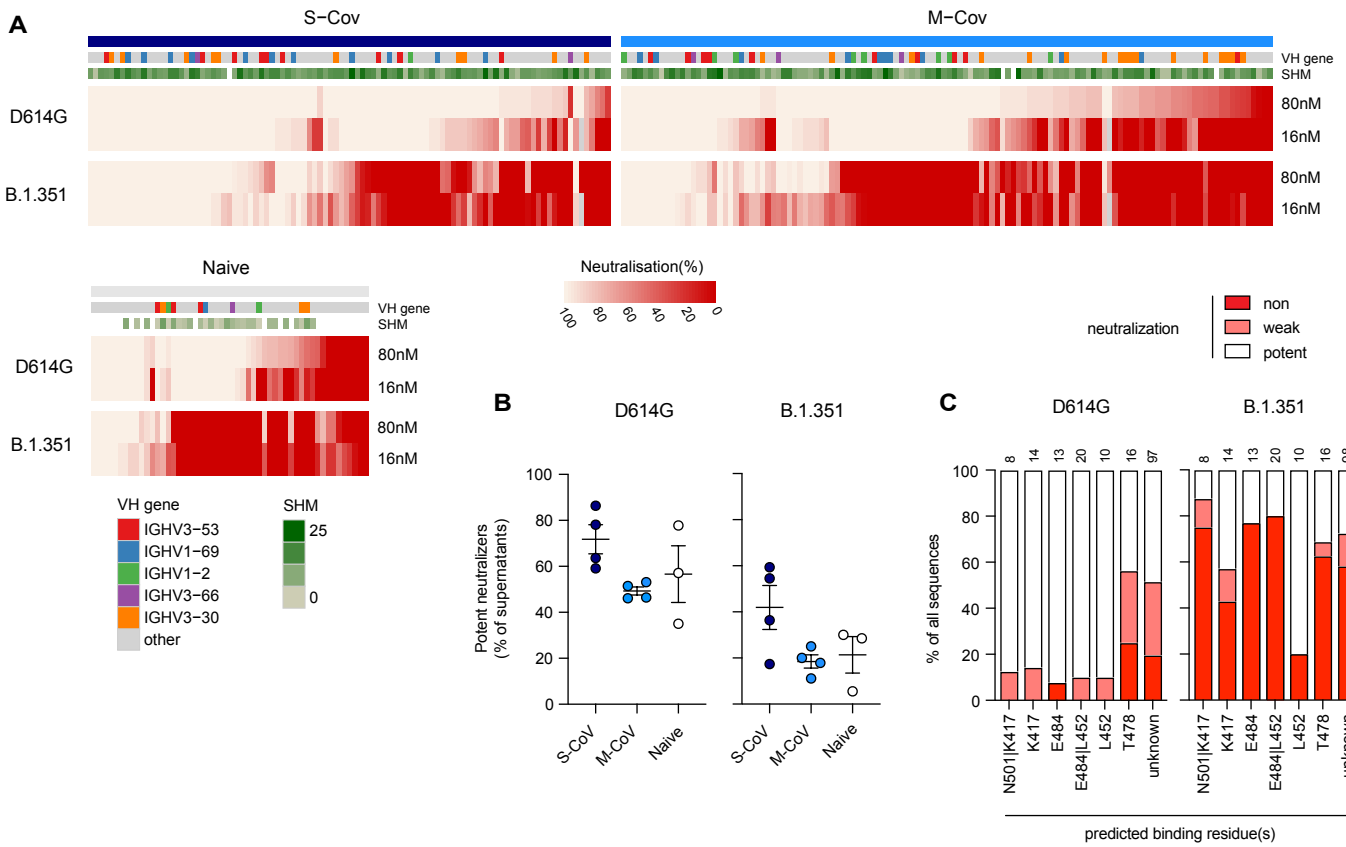


Figure S6: A substantial proportion of memory B cells in vaccinated individuals neutralizes D614G SARS-CoV-2 and B.1.351 VOC. Related to Figure 6.

(A) Heatmap showing the in vitro neutralization of D614G SARS-CoV-2 and B.1.351 SARS-CoV-2 at 80 nM and 16 nM for all tested culture supernatants (S-CoV, n=104; M-CoV, n=123 and naive, n=52). V_H gene name and V_H gene mutation numbers (SHM) for each monoclonal antibody are represented on the top. **(B)** Percentage of potent neutralizers against SARS-CoV-2 D614G or variant B.1.351 viruses among monoclonal antibodies analyzed for each donor. **(C)** Proportion of potent, weak or non-D614G or B.1.351 SARS-CoV-2 neutralizers among all tested monoclonal antibodies, grouped based on their predicted binding residues.